TOWARDS CMOS NUCLEAR MAGNETIC RESONANCE SPECTROSCOPY: DESIGN, IMPLEMENTATION AND EXPERIMENTAL RESULTS

HOSSEIN POURMODHEJI

A THESIS SUBMITTED TO
THE FACULTY OF GRADUATE STUDIES
IN PARTIAL FULFILLMENT OF THE REQUIREMENTS
FOR THE DEGREE OF
MASTER OF APPLIED SCIENCE

GRADUATE PROGRAM IN COMPUTER ENGINEERING
YORK UNIVERSITY
TORONTO, ONTARIO

November 2015

Abstract

Nuclear Magnetic Resonance (NMR) Spectroscopy is used intensively along with other ancillary spectroscopic and characterization techniques. The design and implementation of High Throughput NMR Spectroscopy is a key challenge to accelerate the drug discovery process. On the other hand, the current conventional NMR technologies are expensive and bulky. The development of novel handheld NMR spectroscopy is a key challenge towards NMR spectroscopy for Point-of-Care (PoC) diagnostics applications.

This thesis addresses the above-mentioned challenges of High Throughput NMR Spectroscopy and Handheld NMR spectroscopy by developing new integrated circuits dedicated to NMR spectroscopy using Complementary Metal Oxide Semiconductor (CMOS) technology. Simulation and characterization results were also used to prove the functionality and applicability of the proposed techniques. We have designed two CMOS chips using 0.13-µm technology, first chip includes number of new vertical microcoils and LNA with 780 pV/√Hz at 300 MHz and the second one is a new dual-path NMR receiver.

To My Parents,

For their endless love, support and encouragement

Acknowledgments

I would like to thank my supervisor Prof. Ghafar-Zadeh and co-supervisor Prof. Magierowski for all their supports and encouragements. The implementation of this thesis could not be possible without their advice. Also, I would like to thank Dr. Howard Hunter for his valuable comments on NMR technology. Many thanks to Natural Sciences and Engineering Research Council of Canada (NSERC) for financial support and Canadian Microelectronics Corporation (CMC) for their supports to fabricate, make package, and test our CMOS chip.

TABLE OF CONTENTS

LIST OF TABLES

LIST OF FIGURES

LIST OF ABBREVIATIONS

Analog to Digital Converter	ADC
Complementary Metal Oxide Semiconductor	CMOS
Deep Reactive Ion Etching	DRIE
Deoxyribonucleic Acid	DNA
Differential Stacked Coil	DSC
Digital Signal Processing	DSP
electron-Beam	e-beam
Fast Fast	FF
Focused Ion Beam	FIB
High Frequency Structural Simulator	HFSS
Integrated Circuit	IC
Ion Selective Field Effect Transistor	ISFET
Low Noise Amplifier	LNA
Metal-Insulator-Metal Capacitor	MIM Capacitor
Microcoil	µCoil
Micro-Electro-Mechanical-Systems	MEMS
Microelectronics	µE
Microfluidics	µF
Millimeter Scale Coil	mini-coil
Mixer	MIX

National Institute for Materials Science	NIMS
Nuclear Magnetic Resonance	NMR
Output Differential Amplifier	ODA
Phase Shifter	PS
Point-of-Care	PoC
Polydimethylsiloxane	PDMS
Power Amplifier	PA
Printed Circuit Board	PCB
Radio Frequency	RF
Receiver	Rx
Serial Stacked Coil	SSC
Signal to Noise Ratio	SNR
Slow Slow	SS
Tetramethylsilane	TMS
Three Dimensional	3D
Transceiver	TRx
Two Dimensional	2D
Typical Typical	TT
Variable Gain Amplifier	VGA
Vector Network Analyzer	VNA

LIST OF SYMBOLS

Boltzmann Constant	k
Chemical Shift	δ
Equivalent Capacitance	C_{eq}
Equivalent Inductance	L_{eq}
Equivalent Resistance	R_{eq}
Gyromagnetic Ratio or, Drain Thermal Noise Excess Factor	γ
Input Referred Noise	$v_{n,in}^2$
Isotropic Nuclear Shielding	σ
Larmor Frequency, or Angular Resonance Frequency, or Noise Coefficient	ω_0
NMR RF Magnetic Field	B_1
NMR RF Magnetic Field in *x* Direction	B_{1x}
NMR RF Magnetic Field in *y* Direction	B_{1y}
NMR RF Magnetic Field in *z* Direction	B_{1z}
NMR Signal	$S_{(t)}$
Output Resistance of Transistor	r_o
Part Per Million	ppm
Quality Factor	Q
Resonance Frequency	f_0

Spin-Spin Relaxation Time	T_2
Static Magnetic Field	B_0
Temperature	T
Transistor Transconductance	g_m
Varactor Capacitance	C_v
Voltage Gain	A_v

Chapter 1
Introduction

THE recent advances achieved in standard microelectronics (μE) technologies and their applications to life science sustain a new paradigm in the design and implementation of integrated biosensors. This new breed of devices has recently received significant interest in the variety of challenging fields where they are used to speed up time-consuming analysis and address hitherto, insurmountably difficult tasks such as DNA sequencing [1], cancer detection [2], continuous glucose monitoring [3], in-vitro analysis of neuronal electrophysiology [4] and bacteria growth monitoring [5]. Here, the advantage of standard μE technology, particularly CMOS, lies in its ability to allow a monolithic integration of large numbers of micro-sensors along with their associated electronics circuitry. Fundamentally, this ushers the opportunity to realize a single device capable of replacing an entire chain of classical bio-analysis devices present in contemporary labs. So far,

unpackaged solutions for on-chip analysis have been demonstrated using on-chip sensing techniques as diverse as optical [6], magnetic [7], impedometric [2], capacitive [8]-[9], Ion Selective Field Effect Transistor (ISFET) [10], and NMR modalities [11].

NMR is a powerful method for bimolecular analysis used in a variety of life science applications including drug discovery [12] and PoC disease diagnostics [13]. Among landmark efforts in these directions, Pellecchina *et al* [12] have surveyed the principles that enable NMR for drug discovery applications and Lee *et al* [13] have reported a miniaturized NMR for detecting bacteria with high sensitivity. Despite the great advantages of conventional NMR technologies, these bulky systems are expensive and not suitable for many applications seeking low cost portable sensing techniques. Miniaturization of NMR systems is then a relevant solution to achieve low cost and handheld NMR systems suitable for PoC applications.

1.1 Principle of NMR

NMR is a phenomenon in which nuclei absorb and re-emit Radio Frequency (RF) electromagnetic signal in the presence of a static magnetic field. The spectrum of re-emitted electromagnetic signal contains information of all spins inside the measuring chemical sample [14-15].

An NMR system consists of a coil, a static magnet and an electronics transceiver. Fig. 1.1 shows the schematic of the NMR operation in two phases. In the first phase (Fig. 1.1a), the

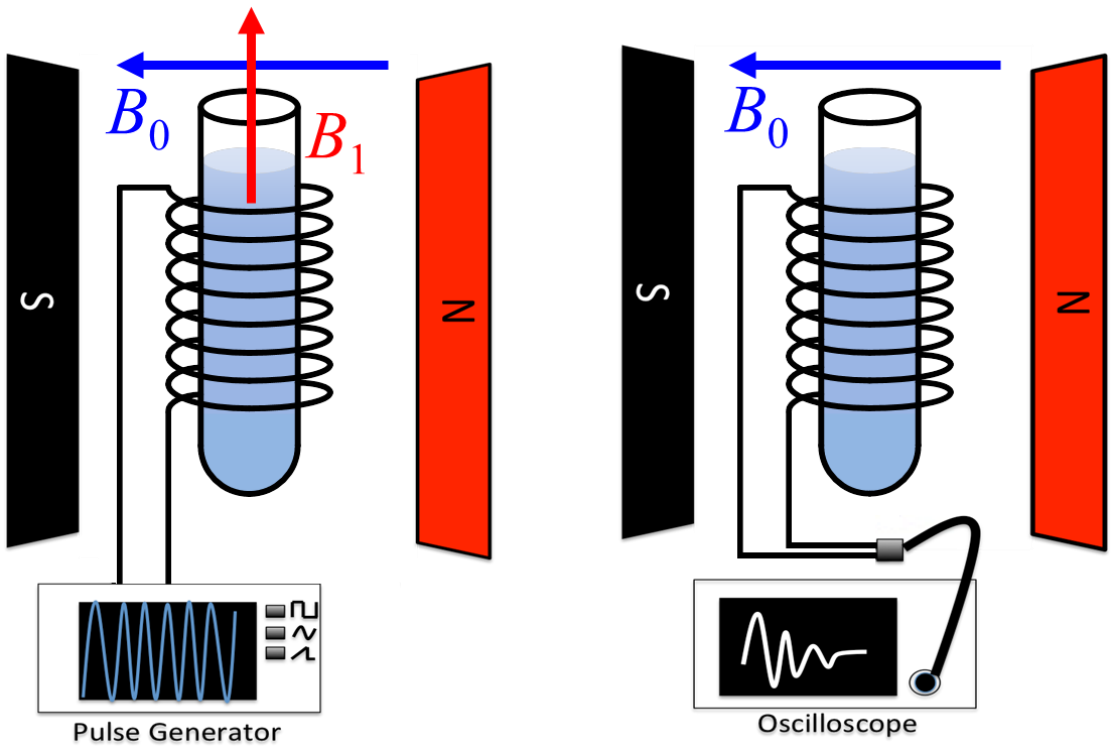

(a) (b)

Fig. 1.1 Illustration of NMR system: (a) excitation mode and (b) recording mode

excitation of the sample is performed and in the second phase (Fig. 1.1b), the re-emitted magnetic signal is recorded. The static magnet field polarizes all nuclei. The RF coil should generate uniform magnetic field B_1. The static magnetic field (B_0) and RF magnetic field (B_1) are perpendicular as seen in Fig. 1.1. This static magnetic field is proportional to the magnetic resonance frequency based on the following equation.

$$\omega_0 = \gamma B_0 \tag{1}$$

Where ω_0 is the Larmor frequency, γ is the gyromagnetic ratio of the nucleus, and B_0 is the static magnetic field. Based on this relationship, a large magnetic field allows the generation and recording the magnetic resonance at high frequency. The frequency of the re-emitted magnetic signal (ω_{sample}) is $\gamma(1-\sigma)B_0$ where the σ is isotropic nuclear shielding of the target molecules. The molecules can be recognized from relative difference between ω_{sample} and ω_0 which is called chemical shift ($\delta = (\omega_{sample} - \omega_0)/\omega_0$).

Signal to Noise Ratio (SNR) of NMR signal can be obtained from the following equation [15].

$$SNR \propto \frac{K \frac{B_1}{i} V_s N \frac{\omega_0^2}{T}}{\sqrt{T \Delta f R_{coil}}} \tag{2}$$

Where K is scale factor of non-uniformity of the RF magnetic field for specific coil, B_1/i is the transverse magnetic field induced in the coil by a unit current, V_s is the sample volume, N is the number of spins per unit volume, T is temperature in Kelvin, Δf is the spectral bandwidth, and R_{coil} is the resistance of the coil. Based on this equation, higher static magnetic field ($\omega_0=\gamma B_0$) results in better sensitivity while higher temperature decreases the sensitivity.

1.2 Conventional NMR System

A commercially available NMR system consists of three parts – static magnetic field generator, NMR probe and a spectrometer. Fig. 1.2 shows the 300 MHz NMR.

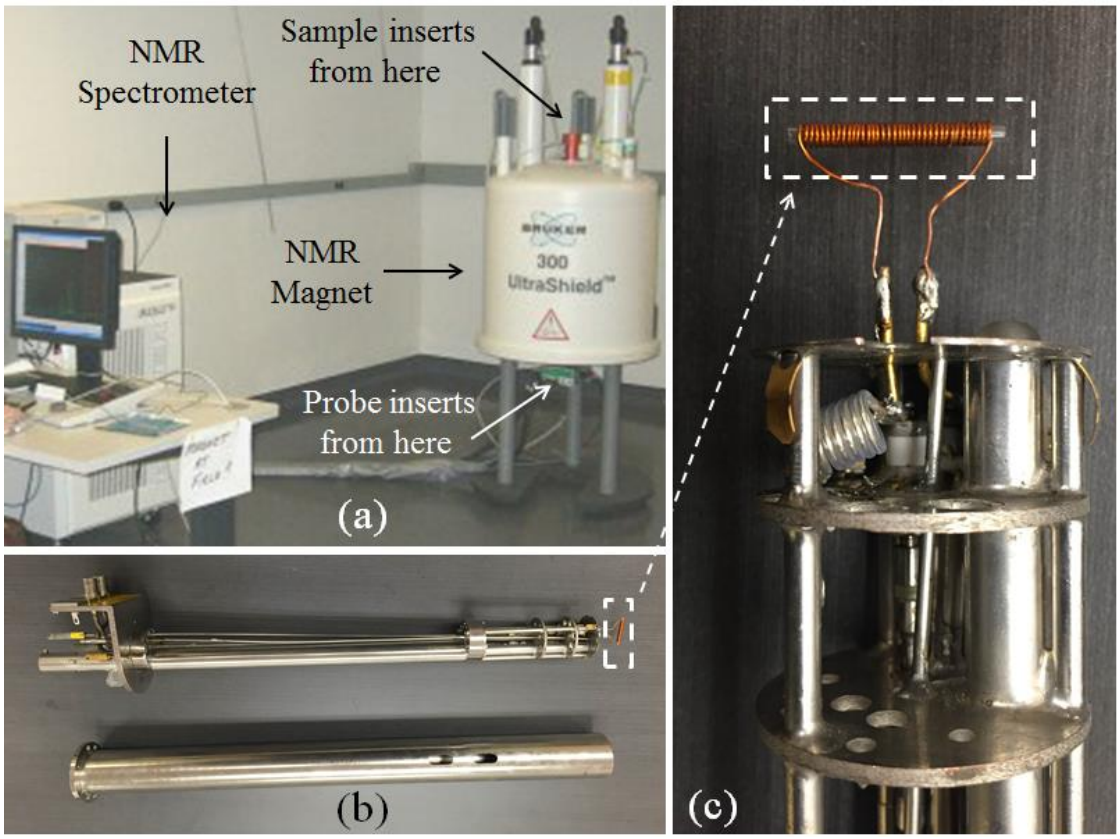

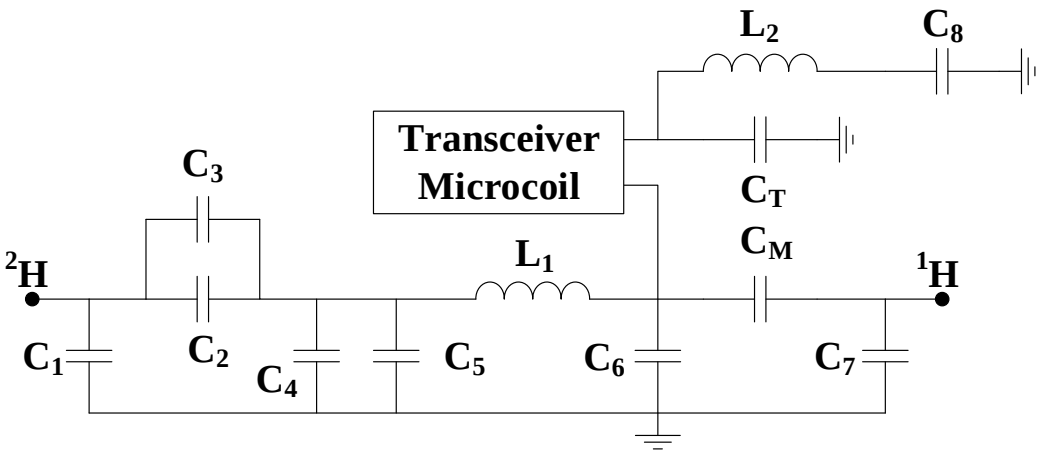

(d)

Fig. 1.2 Conventional NMR System; (a) Photo of 300 MHZ Bruker NMR Magnet and Spectrometer [16], (b) NMR probe, (c) NMR custom made coil connected to NMR probe, and (d) Matching circuit for the Bruker probe

The static magnet is the largest and heaviest component in an NMR system as seen in Fig. 1.2. This figure shows the 300 MHz NMR Bruker located at York University. As depicted in this figure, the large NMR magnet is connected to the spectrometer. As seen in Fig. 1.2b, the NMR probe consists of a coil. Fig. 1.2c shows the custom-made mini-coil wound on a glass tube. As evidenced by Fig. 1.2a, the NMR probe is inserted from the bottom while the sample is inserted from the top into the NMR magnet. Another important part of NMR probe is the matching circuitry. As seen in Fig. 1.2d, variable capacitors are used to accurately match the coil's impedance to 50 Ω coaxial cable's impedance. It is noteworthy that the coil in this network may decrease the SNR due to the presence of resistance in the coils. As shown in Fig. 1.2a, the spectrometer is a bench-top system connected to a computer. This system consists of a transceiver incorporated with a digital signal processing board. The transceiver is an analog circuit consisting of various building blocks such as pulse sequence generator and Low Noise Amplifier (LNA) as seen in Fig. 1.3. As seen in this figure, the front-end block of the transceiver is an impedance matching circuitry to match the input impedance of the transceiver with the 50 Ω coaxial cable connected to the NMR probe. An Analog to Digital Converter (ADC) is the output front-end stage of this transceiver. Fig. 1.3 also shows the digital part of the spectrometer. This part is employed for the NMR signal processing and data acquisition purposes.

As we have mentioned earlier in EQ(1) and EQ(2), the higher magnetic field result in higher resonance frequency and therefore higher resonance frequency increases the SNR.

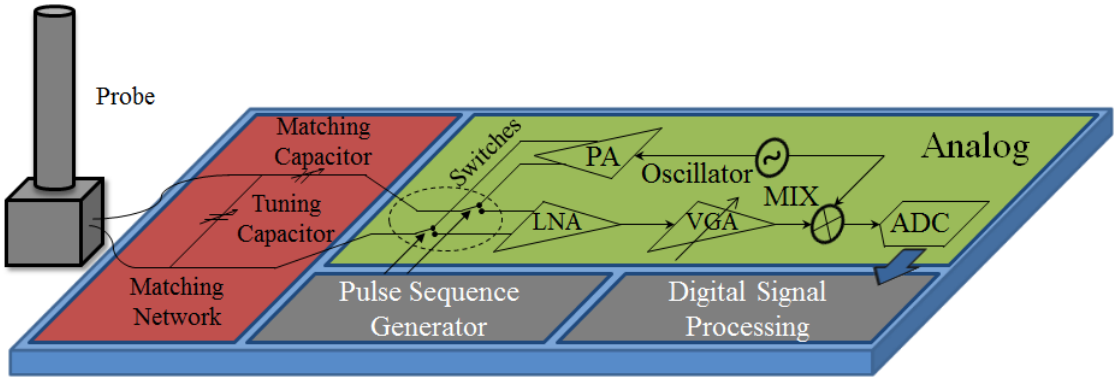

Fig. 1.3 Illustration of spectrometer including three main parts (1) Matching network contains passive components (2) Analog part contains LNA, variable gain amplifier (VGA), mixer (MIX), power amplifier (PA), Oscillator, and ADC (3) Digital part contains pulse sequence generator and digital signal processing (DSP)

However, here is a trade-off between cost of higher magnet and SNR improvement. Based on this fact, Table 1 shows various commercially available NMR systems operating in different resonance frequencies ranging from 2.3 KHz to 1GHz. As seen in this table, thanks to the great advances of NMR technologies, researchers can perform NMR spectroscopy in different frequencies with high SNR. For instance, the National Institute for Materials Science (NIMS) has recently developed a high magnetic station that is used for NMR spectroscopy higher than 1GHz. As seen in this table, many companies including Bruker, Oxford Instrument, GMW, ASG, Magritek and Cryogenic have launched their NMR products in the market. Based on this table, the main challenges of NMR technology are the development of high frequency NMR systems with high SNR.

Table 1: Different commercially available NMR systems

Company	Proton NMR Frequency	B_0 (Field Strength)	References
NIMS	1020 MHz	24 T	[17][18]
Magritek	2.3 kHz	0.54 G	[19][20]
Oxford Instruments	250 MHZ	5.9 T	[21][22]
Bruker	20 MHz	0.47 T	[13][23]
Metrolab Instruments	21.65 MHz	0.5 T	[24][25]
Varian	60 MHz	1.4 T	[26]
Aster Enterprises	41 MHz	0.96 T	[27]
GMW Associates	680 MHz	16T	[28][29]
ASG Superconductors	21 MHz	0.5 T	[30][31]
Qualion NMR.	60 MHz	1.4 T	[32]
Resonance Systems Ltd.	20 MHz	45 T	[33][34]
JEOL USA, Inc.	930 MHz	21.8 T	[35]
SpinCore Technologies, Inc.	11.6 MHz	0.275 T	[36]

1.3 NMR Challenges

Despite great advances of NMR technologies for life science applications, still there are many key challenges to achieve the full potential of NMR technology for life science applications at the single molecule or single atom levels. The sensitivity can be improved in different ways as mentioned below.

1.3.1 Static Magnetic Field B_0

According to EQ. 1, B_0 is a key factor in the design and implementation of highly accurate NMR system. As shown in Table 1, the world largest superconductive magnet is a 24 T magnet that is used in over 1GHz NMR spectroscopy systems. It is noteworthy that the emerging NMR systems using small magnet with lower B_0 intrinsically suffer from a low sensitivity that should be improved. In the chapter 2, we address a new circuit may improve the SNR.

1.3.2 Low Temperature NMR

As already it is mentioned, lowering the temperature is the key in the design and implementation of novel high-SNR NMR systems. This includes the temperature of the sample, coil and microelectronics circuitry. For this purpose, several companies such as Cryogenic Ltd have launched new NMR systems offering very low temperature operation. Indeed the thermal noise of the coil, sample and transceiver is around 20 K. Despite the fact that in such a NMR technology, the transceiver along with the NMR probe are placed in a chamber with the low temperature, the circuit techniques have also been used in the transceiver design in order to further cancel the effect of thermal as well as flicker noise generated in the circuit.

1.3.3 Filling Factor

The filling factor is the ratio of the sample's volume to the volume of the space exposed to the uniform magnetic field of the RF coil [14]. This definition is widely used in the NMR related literature. A higher filling factor can be achieved by developing coils with specific geometry surrounding the sample. Indeed, if the size of coil is larger than sample, the NMR signal cannot be measured accurately. Therefore, the design and implementation of RF coil and sample holder with the maximum filling factor is a challenge. This goal might be achieved by lowering the size of coil. Indeed by developing small coils with the same size of sample both requirements of low sample consumption and high filling factors can be met. According to the reciprocity principle which is described by Hoult, the sensitivity of the NMR RF coil is inversely proportional to its diameter, when the length to diameter of that coil is constant [14, 37]. Based on this, the miniaturization of the coil is a challenge to increase NMR sensitivity [38]. In order to improve the filling factor, the novel sample holder and microfluidics should be developed that is not the focus of our research in this thesis. For this reason we will not discuss about the improvement of the filling factor in this thesis.

1.3.4 Miniaturization of RF Coil

Despite great advantage of conventional NMR systems for life science applications, these systems are heavy, bulky and expensive and not suitable for many Point-of-Care diagnostics applications requiring handheld or portable systems. On the other hand, the

miniaturized NMR system holds great promise as high SNR NMR devices suitable for drug discovery applications. As shown in Table 2, to date, several attempts have been made toward miniaturization of NMR.

As seen in Table 2, in addition to solenoid coil, other geometries such as, Helmholtz [39-40], planar coil [41] (using liquid metal [24]), Stripline [42] and micro-slot [43] have been reported in new NMR systems. The main challenge in these works is to increase the quality factor (Q). The quality factor is defined as the ratio of reactance of the coil over its parasitic resistance ($L\omega/R$). This table shows the achieved Q and/or related R in each reported NMR recording/excitation device. Based on EQ(2), these parameters have effect on the NMR SNR. Despite this fact that the uniformity of B_1 is very crucial, less attentions have been paid to develop such devices with specific geometries to generate uniform B_1 over micro-scale samples. Among various geometries techniques, planar micro-coil has been reported by a number of researchers for NMR application. This is because of low complexity of required micro-fabrication process (such as photolithography [54]) and integrability with standard microelectronics technologies such as CMOS as described later in this chapter.

1.3.5 CMOS NMR

For the past several decades CMOS technology has played a significant role in computer systems and mobile communication. The landmark RF CMOS for mobile communication inspired the idea of developing NMR system on chip. CMOS technology by offering a

Table 2: Miniaturized NMR systems

Frequency	Magnet	Coil Specifications	Miniaturized Coil	Spectrometer Specifications	References
20.9 MHz	0.49 T	Q = 1.9	CMOS Planar microcoil	CMOS Fully Integrated Rx	[11]
21.65 MHz	0.5 T	R = 0.3 Ω Q = 30.4	Planar Microcoil Liquid Metal	Off-chip Spectrometer	[24]
60 MHz	1.4 T	Q = 42	Planar Microcoil Sensonit Microfluidics	Off-chip Spectrometer	[26]
300 MHz	7 T	Q = 8	CMOS Planar microcoil	CMOS Fully Integrated Rx	[38]
61 MHz - 400 MHz	9.4 T	R = 7 Ω	Planar Microcoil Sensonit	Off-chip Spectrometer	[41]
500 MHz	11.7 T	Q = 256(LC)	Microslot	Off-chip Spectrometer	[44]
500 MHz	11.7 T	R = 0.03	Microslot	Off-chip Spectrometer	[45]
85.13 MHz	2 T	Q = 7	Planar microcoil	CMOS Fully Integrated Rx	[46]
300 MHz	7 T	Q = 6	CMOS Planar microcoil	Fully Integrated Rx	[47]
21.3 MHz	0.5 T	Q = 16	Off-chip Planar microcoil	CMOS Fully Integrated Rx	[48]
300 MHz	7 T	R = 0.46 Ω	Solenoid	Conventional NMR spectrometer (Bruker DRX 300)	[49]

300 MHz	7 T	R = 0.55 Ω	Planar coil	Conventional NMR spectrometer (Bruker DRX 300)	[49]
300 MHz	7 T	R = 1.52 Ω	Helmholtz coil	Conventional NMR spectrometer (Bruker DRX 300)	[49]
< 400 MHz	7 T	N/A	N/A	Off-chip OPENCORE NMR spectrometer	[50]
85 MHz	2 T	R = 1.8 Ω	Laser direct-write lithographic technique	Custom made spectrometer from Tecmag Inc	[51]
23.9 MHz	0.56 T	Q = 28	Solenoid Microcoil	CMOS Fully Integrated Rx	[52]
600 MHz	14.1 T	Q = 80~100	Stripline RF coil	Chemagnetics CMX-Infinity 600 solid-state NMR spectrometer	[53]

distinct cost, highly integrated circuits and micro-scale coils is the best candidate for the design and implementation of active NMR system as mentioned below. Also, it is noteworthy that the CMOS by offering very high accurate circuitry can play important role in improving SNR by developing new circuitry.

In this direction, T. Cherifi [46] took the first step in 2005 by developing a CMOS microcoil-associated preamplifier for NMR spectroscopy, then Hakho Lee [13] in 2008 introduced the first chip-NMR biosensor for detection and molecular analysis of cells. In the meanwhile, another group [55] was working on miniaturized NMR system. Jens Andres *et al* [55] in 2008 have developed a low-noise CMOS receiver front-end for NMR applications. As the follow up of these works, we design CMOS chip featuring LNA as described in chapter 2 and 3.

In our thesis, the main role of CMOS is to develop RF circuit suitable for high throughput NMR as mentioned in chapter 2. Another role of the CMOS is development of the novel RF circuitry associated with dual path technique as mentioned in chapter 3.

1.4 Objectives and Organization of Thesis

The focus of this research is placed on the design and implementation of CMOS integrated circuits dedicated to NMR spectroscopy. In this thesis, two important challenges of NMR technologies are addressed. These challenges are High Throughput Spectroscopy as well as low frequency (or low magnetic field) NMR spectroscopy. The outcome of this research results in innovative NMR technologies that can be used for drug discovery and PoC diagnostics applications.

1) High Throughput NMR Spectroscopy: High Throughput NMR system features a number of coils for multiple NMR spectroscopy purposes. Despite great advances of NMR

technologies, the challenge of the development of High Throughput NMR spectroscopy remains unmet and no commercial High Throughput NMR system is available in the market. In this approach, the design and implementation of NMR probe with a large number of RF coil along with associated circuitries are discussed. You can see the conventional NMR probe and the new proposed one in Fig 1.4a and Fig. 1.4b, respectively. We will talk about this approach in chapter 2 in details.

2) Low frequency NMR spectroscopy: As already mentioned, the lower B_0, the lower SNR is expected. Therefore, the SNR should be improved using lower RF magnet or other circuit technique. In this direction, this thesis present a novel dual path receiver dedicated to NMR spectroscopy. *Chapter 3* describes a new circuitry designed and implemented using CMOS process.

Chapter 2 addresses the first challenge by proposing a novel on-chip vertical micro-coil incorporated with low noise readout circuitry. The Cadence and High Frequency Structural Simulator (HFSS) simulation results are demonstrated and discussed in order to prove the functionality and applicability of proposed integrated circuit.

Chapter 3 describes a dual path NMR receiver designed and implemented using 0.13-µm CMOS process. This receiver comprises a CMOS chip connected to mini-coils for NMR spectroscopy purposes. This chapter describe and demonstrate the Cadence and HFSS

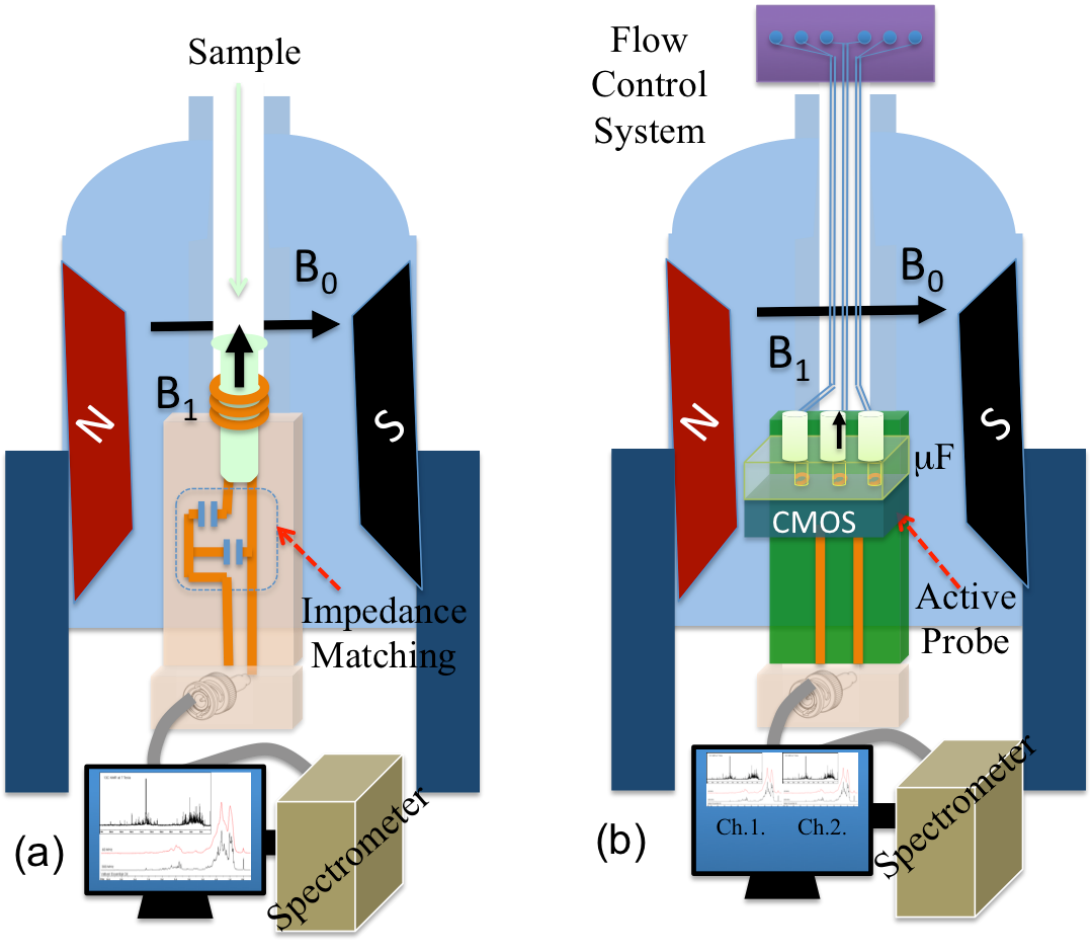

Fig. 1.4 NMR Spectroscopy: Illustrations of NMR system with a) passive NMR and b) active probe (μF=Microfluidics)

simulation results. Also, the CMOS chip characterization results are shown in this chapter.

Chapter 4 presents a summary of the proposed techniques and research results achieved results. This thesis takes the first step toward the development novel NMR technologies. The continuation of this work in the future in order to develop fully functional NMR spectroscopy is also discussed.

Chapter 2
300 MHz CMOS NMR Probe

In this chapter, the design and simulation of a 300 MHz CMOS NMR probe is demonstrated and discussed. The main goal of this study is to take the first step towards the development of High Throughput NMR Spectroscopy. Fig. 1.4 compares the proposed High Throughput NMR system with a conventional NMR system consisting of a passive probe. This passive NMR probe comprises of a RF coil surrounding the sample and a matching network between the coil and spectrometer. Fig. 1.4b illustrates an active NMR probe consisting of a CMOS chip. This single chip features a number of coils associated with underneath conditioning circuitries. In this chapter the proposed circuit and sensor (μCoil) are presented.

2.1 µCoils

CMOS technology, by offering multiple metal layers, is the best candidate to design three dimensional (3D) µCoils with specific geometry suitable for high SNR NMR spectroscopy. In this section, we demonstrate and discuss the design and simulation results of two different µCoil structures, namely: serial stacked coil (SSC) and differential stacked coil (DSC) shown in Fig. 2.1a and Fig. 2.1b.

2.1.1 SSD and DSC Structures

SSC is a simple structure consisting of multiple planar coils in different metal layers indexed by i where $8 \geq i \geq 1$, because 0.13-µm CMOS technology that we are using, includes 8 metal layers.

These planar coils with several turns indexed by j, where n≥.j≥1 are connected through vias in order to realize a large inductance as seen in Fig. 2.1c. Best on our HFSS simulation the optimum value of n is equal to 9 for the best quality factor around 300 MHz. However the equivalent resistance will be increased as expressed in EQ. 3 [56-58]

$$R_{eq-SSC} = \sum_{i}\sum_{j} R_{i,j} \tag{3}$$

The DSC is a symmetrical differential structure consisting of multiple planar µCoils (i layers, and j turns in each layer) that are connected to each other with two vias [58-59]. The equivalent resistance of a DSC structure is expressed in EQ. 4

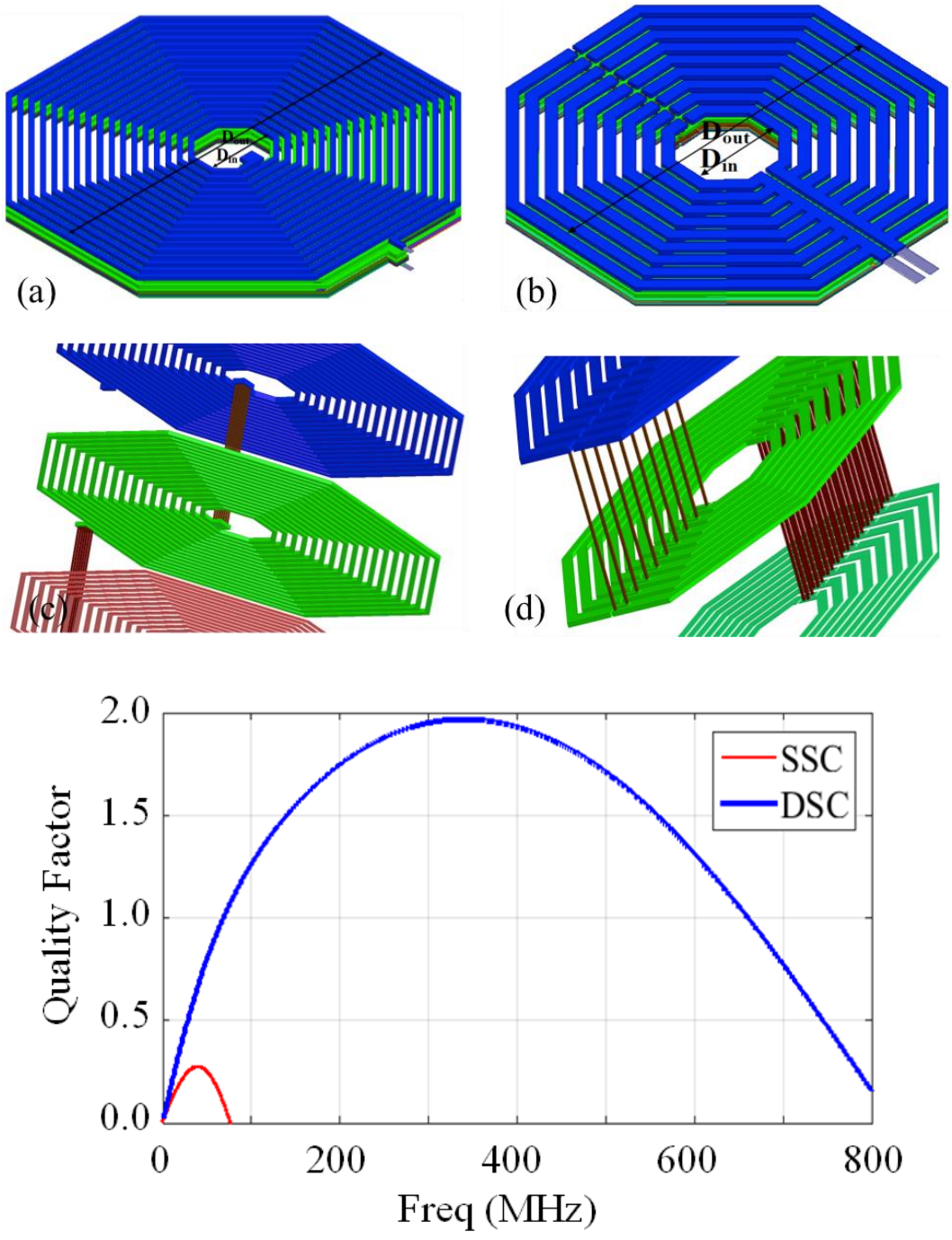

(e)

Fig. 2.1 NMR µCoil structures: (a), (c) SSC, (b), (d) DSC and (e) Quality factor results of both DSC and SSC structures

$$R_{eq-DSC} = \sum_{i}\left(\sum_{j} R_{i,j}^{-1}\right)^{-1} \quad (4)$$

As described in [58], in our design, each layer is a multiple parallel coil in order to increase the magnetic field B_1 and decrease resistance. Therefore, a number of vias are used in parallel to connect the µCoils between two layers as seen in Fig. 2.1d.

The equivalent circuit model of both DSC ad SSC structures is a tank circuit and therefore the quality factor of their equivalent circuits can be expressed by

$$Q_{L(\omega)} = \frac{\omega L_{eq}}{R_{eq}}\left(1 - \frac{C_{eq}R_{eq}^{\ 2}}{L_{eq}} - \omega^2 L_{eq}C_{eq}\right) \quad (5)$$

Where L_{eq} and C_{eq} are the equivalent inductance and capacitance and R_{eq} is the equivalent resistance that can be obtained from EQs. 3 or 4 for SSC and DSC structures, respectively. Based on EQs. 3-5, one can roughly conclude that the quality factor of the DSC structure is higher than that of the SSC structure. This is because $R_{eq\text{-}SSC} >> R_{eq\text{-}DSC}$. In the next section 2.1.2, we calculate the quality factor using a finite-element electromagnetic simulator (ANSYS HFSS).

2.1.2 Geometry Design, Modeling and Optimization

Two different topologies of the stacked inductors (DSC and SSC) are designed in a CMOS compatible manner using 8 metal layers. In this design, from a circuit point of view, two parameters are important for the design of µCoils. These parameters are the self-resonant

frequency f_0 and the quality factor, which determines the noise level of the µCoil. Additionally, in the design of µCoils, the silicon area is another very important factor that should be minimized.

The ANSYS HFSS software is employed to search for an optimum geometry at f_0 = 300MHz. Based on these studies, the quality factors of both structures versus frequency is obtained as shown in Fig. 2.1e. The optimum inner and outer dimensions of the hexagonally shaped DSC structure are 80 and 365 µm, respectively. The same geometry was also used for the SSC structure. As the results of HFSS modeling and simulation, the operating frequencies of SSC and DSC structures are 40MHz and 300MHz, respectively as seen in Fig. 2.1e. As expected (see 2.1.1), due to the DSC's differential configuration, the inductor's quality factor is around 2, a value 7X better than the SSC structure's quality factor.

2.1.3 Homogenous Magnetic Field

Another advantage of the DSC structure is the homogeneity of the magnetic field B_1 generated inside the µCoil. As seen in both structures (see Fig. 2.1c and Fig. 2.1d), the metal vias introduce horizontal magnetic field components which affect on the homogeneity of the magnetic field B_1. In the DSC structure, the current flowing through the vias between any two layers is oriented in opposite directions.

These opposite current directions almost cancel the horizontal magnetic field components. Therefore, one can argue that the symmetric structure of the DSC can largely cancel the magnetic parasitic effects while the asymmetric structure of SSC cannot.

The magnetic field generated by these asymmetric and symmetric structures in three different directions (B_{1x}, B_{1y} and B_{1z}) are demonstrated in Fig. 2.2a to Fig. 2.2f. As seen in these figures, the magnetic field in *x* and *y* directions are less than the magnetic field in *z* direction in both DSC and SSC structures in the middle of the coils. The ratio of the B_{1xy} over B_{1z} is 3.02% (33.67/1114) at the center point of the SSC while this ratio is 0.93% (11.89/1274) at the center point of the DSC. Based on these values, the vertical magnetic field B_{1z} in both structures are close to each other while the DSC has lower magnetic field in *xy*-plane in comparison to the SSC structure. In addition, you can see the distribution of the B_{1z} in the middle volume of the DSC and SSC structures, in Fig. 2.3a and Fig. 2.3b, respectively. Based on these results, the mean values of the B_{1z} for the DSC and SSC are 1290 A/m and 1115 A/m, respectively. Furthermore, the standard deviation of the DSC is around 59.5 which is about half of the standard deviation of the SSC (108). Based on all these results, we can say that the uniformity of the magnetic field in the DSC structure is much better than that of the asymmetric structure. This is the key advantage of the DSC structure for NMR spectroscopy.

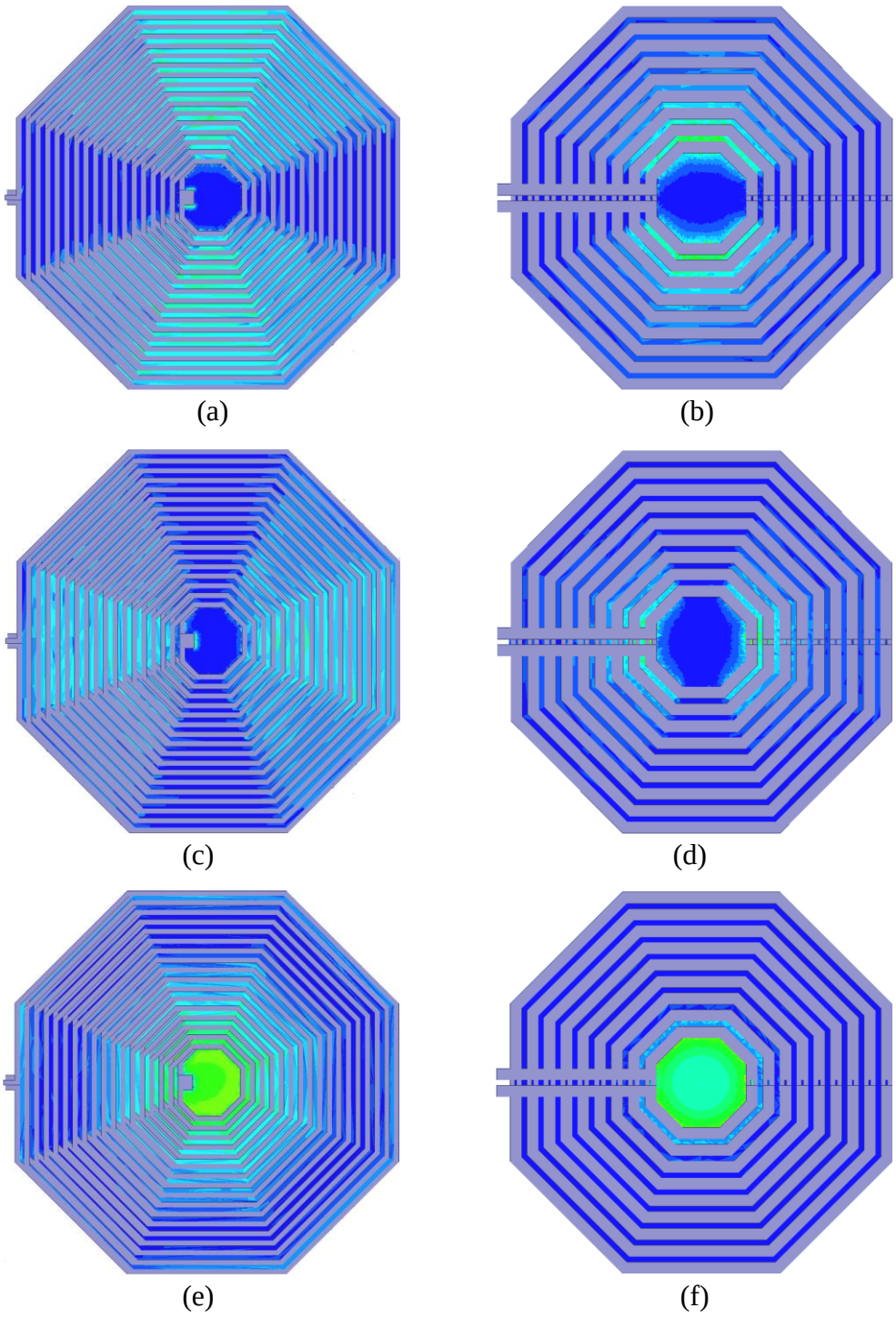

Fig. 2.2 Magnetic field (B_1) simulation results: (a). (c), (e) B_{1x}, B_{1y}, B_{1z}, generated by SSC respectively, (b), (d) and (f) B_{1x}, B_{1y}, and B_{1z}, generated by SSC and DSC respectively.

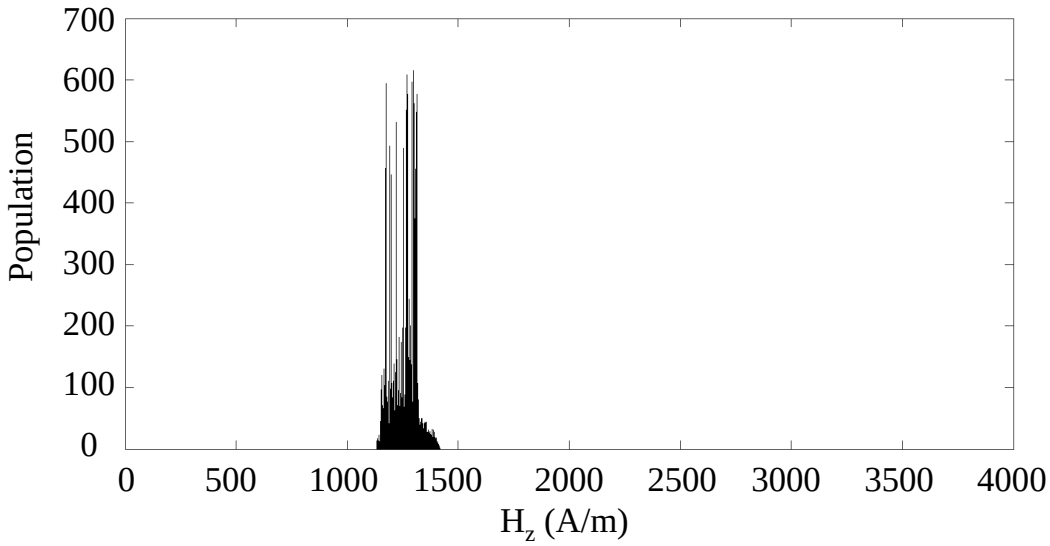

(a)

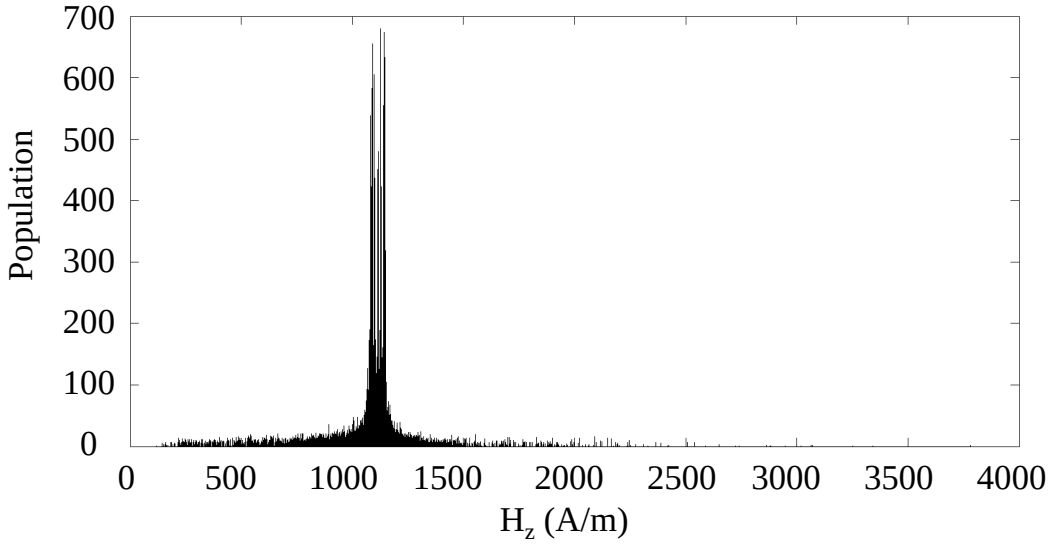

(b)

Fig. 2.3 Population of magnetic field strength (a) DSC (b) SSC

2.2 Low Noise Signal Amplifier

The design of the low noise amplifier is the key factor for the development of high SNR NMR spectroscopy (See section 4.1). A low noise amplifier system consists of two parts; a pre- and a post-amplifier stage.

2.2.1 Front-End Pre-amplifier

It is very crucial to replace the impedance matching with a passive voltage amplifier as reported in [60]. The conventional matching network may decrease the SNR due to the presence of resistance, however, by assuming that LNA has high input impedance, we can remove this conventional matching network and use passive amplifier. Fig. 2.4a shows the circuit model of such a passive voltage pre-amplifier, in essence a series-equivalent resonant circuit. Physically, this LC resonator consists of an on-chip DSC inductor in parallel with a tuning capacitor. The signal induced by the sample is modeled as a voltage in series with the inductor and capacitor pair. A Metal-Insulator-Metal (MIM) capacitor available in the CMOS process is employed to realize the tuning capacitor. By assuming that the LNA's input impedance is very high, the voltage gain of this per-amplifier can be obtained from the following equation.

$$|A_v| = \frac{1}{\sqrt{\left(1 - LC\omega^2\right)^2 + \left(R_S C\omega\right)^2}} \tag{6}$$

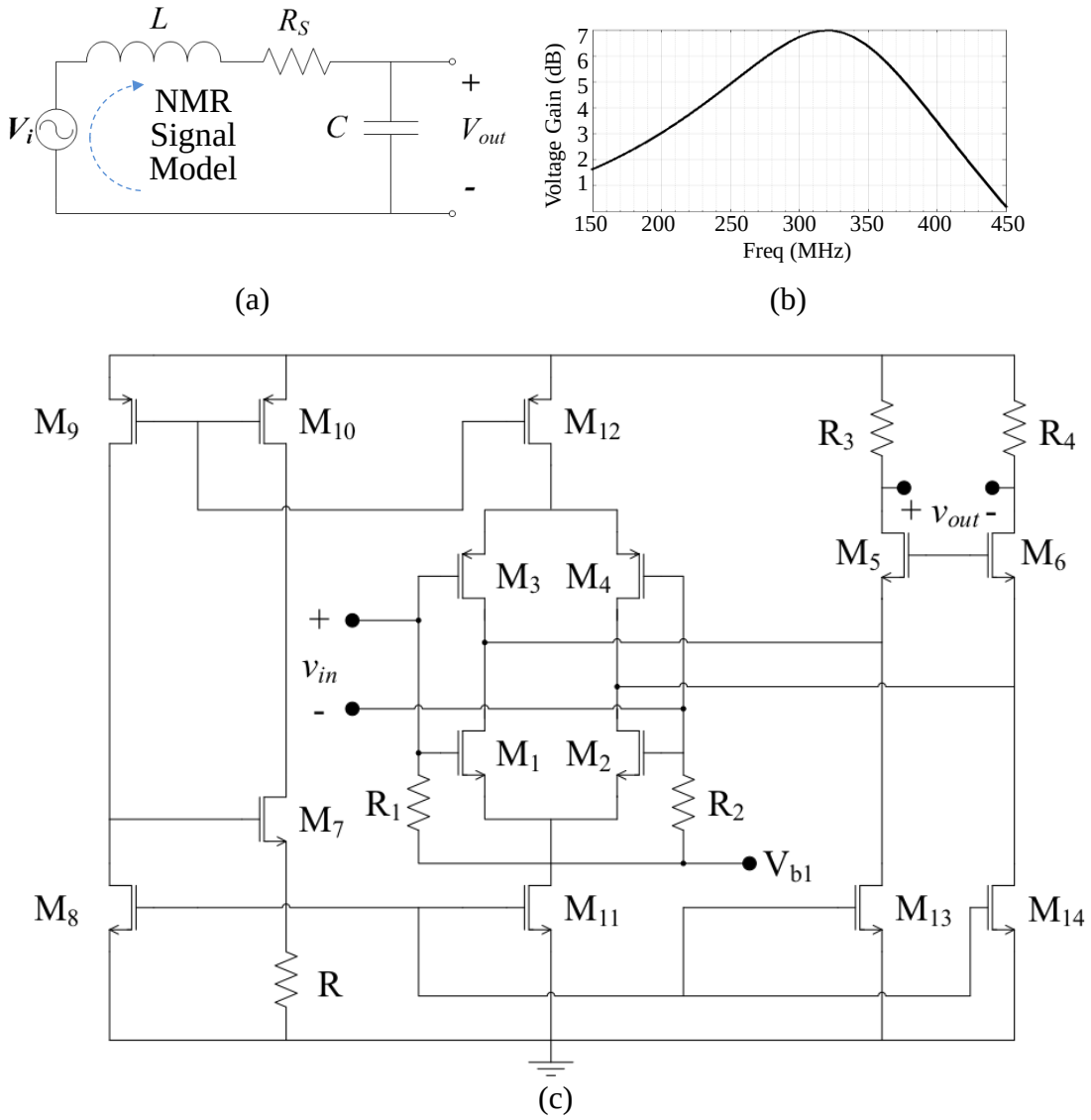

Fig. 2.4 Low noise amplifier (a) Per-amplifier equivalent circuit (b) Voltage gain of preamplifier, (c) Schematic of LNA circuitry.

The optimum capacitance can also be obtained by taking the differential of EQ. 6 at C ($\partial|A_v|/\partial C = 0$)

$$C = \frac{L}{\left(L\omega\right)^2 + {R_S}^2} \tag{7}$$

Therefore, by choosing *C*, the voltage gain becomes maximum as shown in Fig. 2.4b, at a frequency around 300MHz. Indeed this input LC structure (pre-amplifier) boosts the weak NMR signal with minimal noise corruption for ensuing signal processing. This pre-amplification is followed by a post amplifier shown in Fig. 2.4c and described in 2.2.2.

2.2.2 Front-End Post-amplifier

The post-amplifier is a fully differential cascode push-pull LNA that is designed and implemented for NMR spectroscopy purposes [47]. In this circuit M_1-M_4 serve as the core of the LNA and constitute a differential cascode voltage amplifier circuit to suppress the common mode noise. In this sub-circuit, M_1-M_2 are NMOS and M_3-M_4 are PMOS transistors. The total voltage gain can be obtained from

$$\left|A_{v-LNA}\right| = \left(g_{m1} + g_{m3}\right)R_3 \tag{8}$$

Where g_{m1} and g_{m3} are the transconductances of the NMOS and PMOS input transistors and $R_3 = R_4$ are the output resistive loads. M_7-M_{12}, R and $R_1 = R_2$ constitute a bootstrap voltage reference's circuitry to regulate the bias of the amplifier. This circuitry is used to minimize the thermal effect on the circuitry's biasing. On the other hand, M_{13}-M_{14} as well as M_{11} mirror the bias currents of M_8.

For noise performance, we need to optimize the noise source of $M_{1\text{-}4}$. According to the circuit shown in Fig. 2.4c, the input referred noise due to M_1 and M_3 can be stated as follows

$$\overline{v_{n,in}^{\,2}} = 8kT\gamma\left(\frac{1}{g_{m1}+g_{m3}}\right)+4kT\left(\frac{1}{\left(g_{m1}+g_{m3}\right)^2 R_3}\right) \tag{9}$$

Where T, k and γ are temperature in Kelvin, Boltzmann constant and the drain thermal noise excess factor respectively. Based on this equation, the noise can be reduced by increasing the DC currents or, equivalently, g_{m1} and g_{m3}. However the extra DC current increases the power consumption and consequently the temperature resulting in higher thermal noise level. In other words, by designing a low power circuit, we can prevent the self-heating of the chip [47].

2.3 LNA Post-layout Simulation

We thereafter designed the layout of the integrated circuit (see Fig. 2.5) and performed the simulations. In this layout, the HFSS μCoil model was transferred to the Cadence IC design suite and connected to the amplifier.

As we discussed in 2.2.2, the LNA is designed for optimum input referred noise. Therefore, we designed the LNA with a large transconductance for the input transistors to achieve about 780 pV/√Hz at 300 MHz. Fig. 2.6a shows the input referred noise of the LNA for three fabrication process corners. Another important parameter of the LNA is

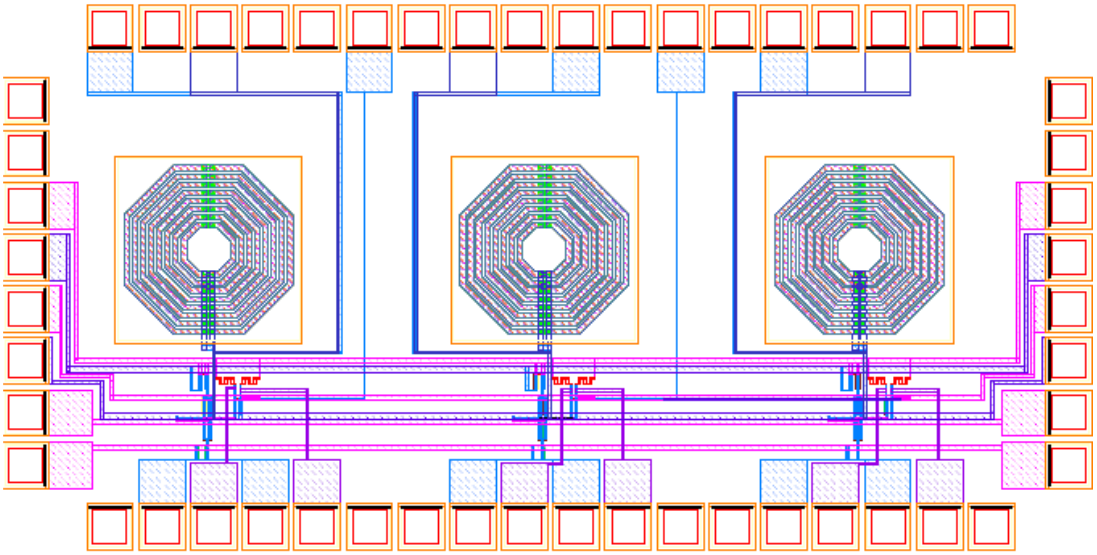

Fig. 2.5 CMOS layout revealing three coils and associated per- and post-amplifiers.

the voltage gain. The voltage gain of the front-end receiver is around 43 dB at 300 MHz and this voltage gain for three fabrication process corners is shown in Fig. 2.6b. Also, both the input referred noise and the voltage gain of the front-end receiver are simulated for temperature variation (-60 $^{\circ}$C to +60 $^{\circ}$C) and shown in Fig. 2.6c and Fig. 2.6d for three fabrication process corners, respectively. It is noteworthy to mention that the bandwidth of the NMR signal is in the range of kHz.

2.4 Spectral Analysis

According to the Bloch equations [61], the NMR signal $S_{(t)}$ over time should be as below

$$S_{(t)} = S_{(0)} e^{j\omega_0(1-\sigma)} e^{-t/T_2} \tag{10}$$

$$S_{(0)} \propto M_{eq} \tag{11}$$

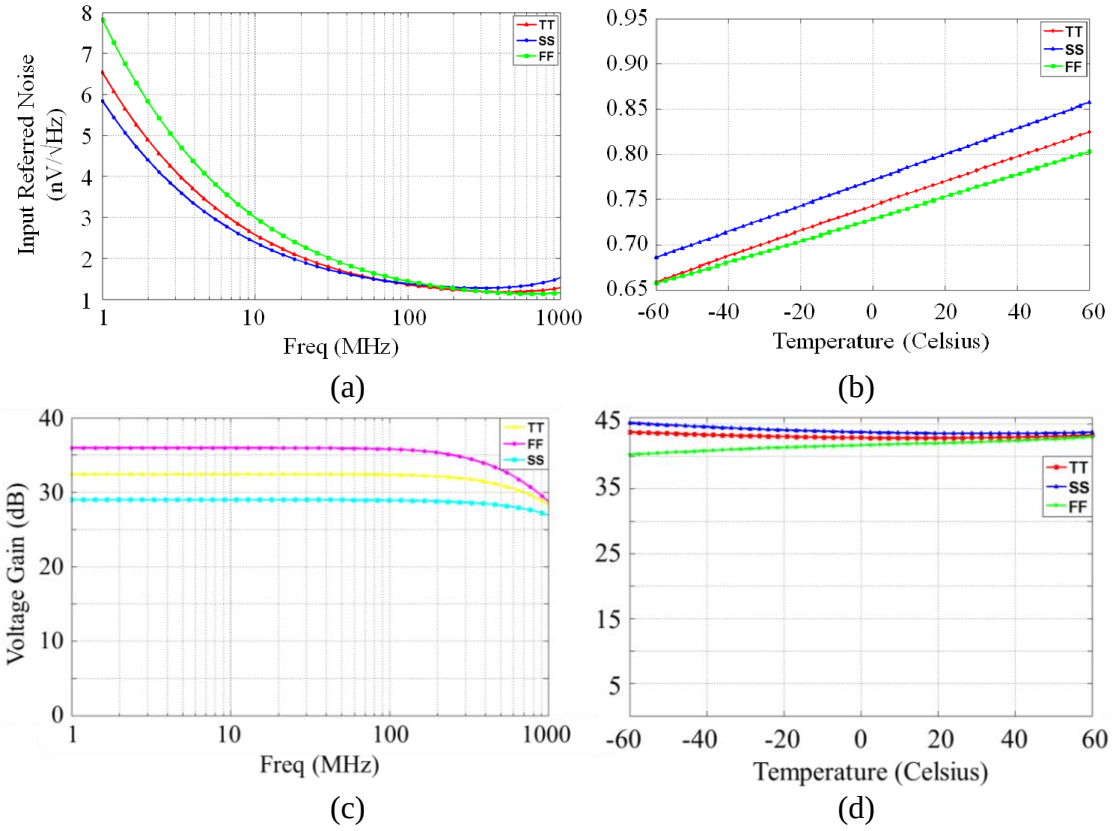

Fig. 2.6 Simulated input referred noise of the (a) LNA over frequency and (b) the LC-LNA over temprature at 300 MHz for three fabrication process corners. Simulated voltage gain of the (c) LNA over frequency and (d) the LC-LNA over temperature at 300 MHz for three fabrication process corners

Where ω_0 is the angular resonance frequency, σ is isotropic nuclear shielding, and T_2 is the spin-spin relaxation time. Also $S_{(0)}$ indicates the NMR signal just before the excitation and M_{eq} is nuclear magnetization amplitude of the sample proportional to the number of spins per unit volume (N) and B_0. In this part, two NMR signals are modeled for the -CH3 group of Lactate and Creatine (Cr). For the first one the chemical shifts are 1.27 and 1.39 ppm

and for the latter one it is 3ppm related to the reference frequency of 300 MHz. T_2 is almost 1040 mS and 100 mS, respectively.

By using these values, we can model the NMR signal, which we use as the input of our LNA. If we consider that the bandwidth of the signal is 1.1 kHz for the purpose of noise calculations, and the parasitic resistance of the coil is 10 Ω, then the corresponding output spectra of both signals relative to the reference frequency of 300 MHz are shown in Fig. 2.7a and Fig. 2.7b, respectively. The simulation results for water and toluene in the time domain and frequency domain are shown, as well. According to [62], water (H_2O) has one chemical shift (δ) of 1.588 ppm and toluene (C_7H_8) has two chemical shifts of 2.34 ppm and 7 ppm. If we use EQs.10-11, we should find the relative isotropic nuclear shielding from associated chemical shift

$$\delta_{sample} = \frac{\sigma_{ref} - \sigma_{sample}}{1 - \sigma_{ref}} \tag{12}$$

According to EQ. 12, if we consider tetramethylsilane (TMS) as the standard reference whose chemical shift and isotropic nuclear shielding are zero, then we can derive the σ from the specific chemical shift. By this and (EQs. 10-11), the output signal of our circuit for water and toluene in both the time domain and frequency domain can be obtained as shown in Fig. 2.8 and Fig. 2.9.

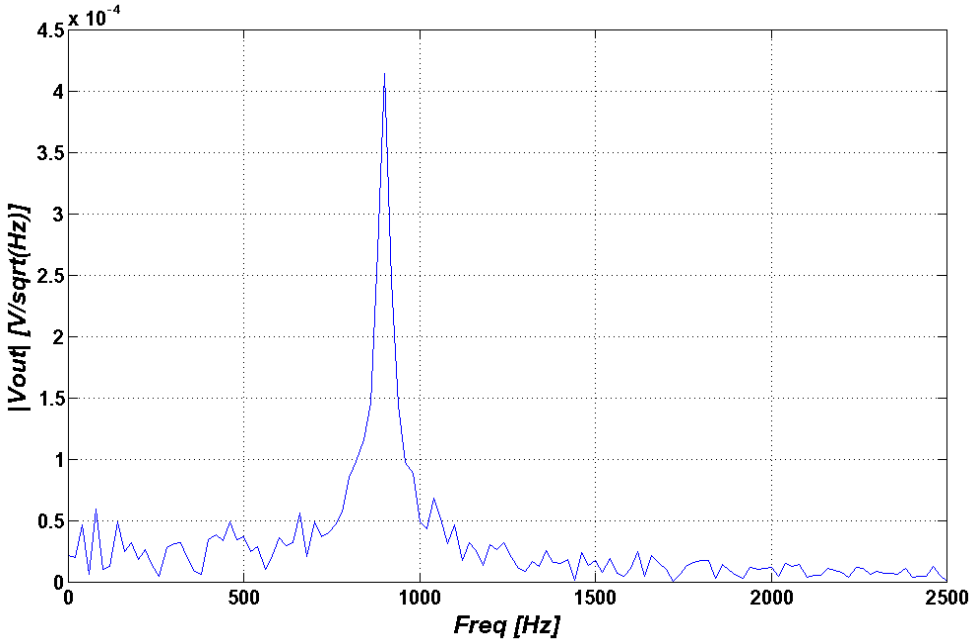

(a)

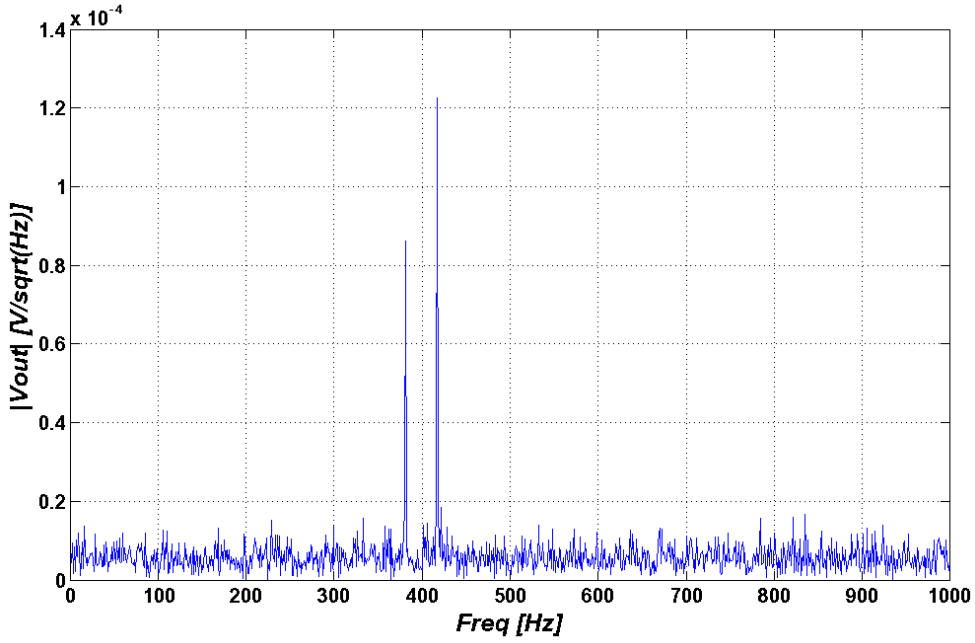

(b)

Fig. 2.7 Simulated NMR spectrum for (a) -CH3 group (b) Creatine group.

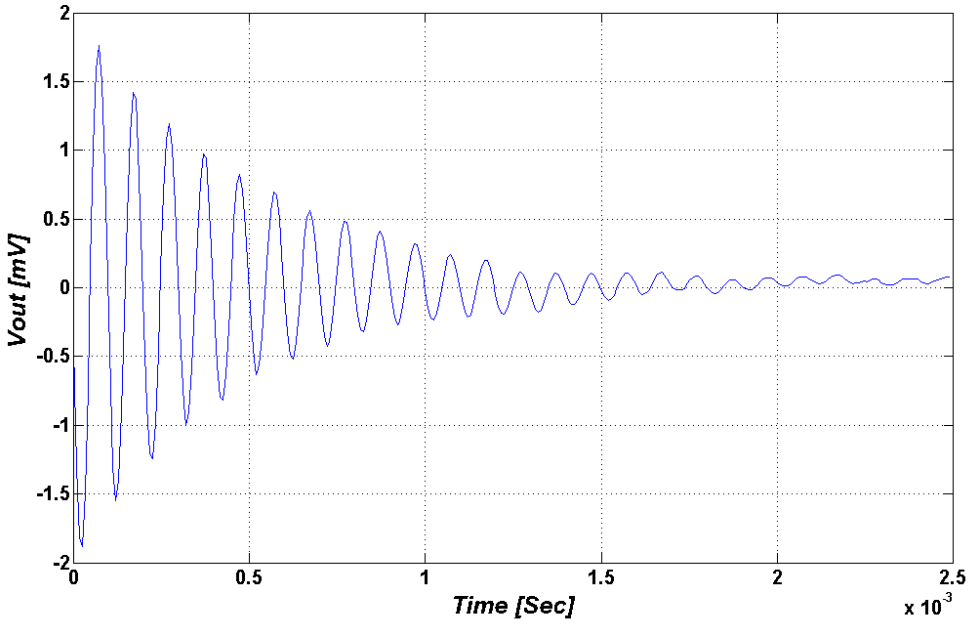

(a)

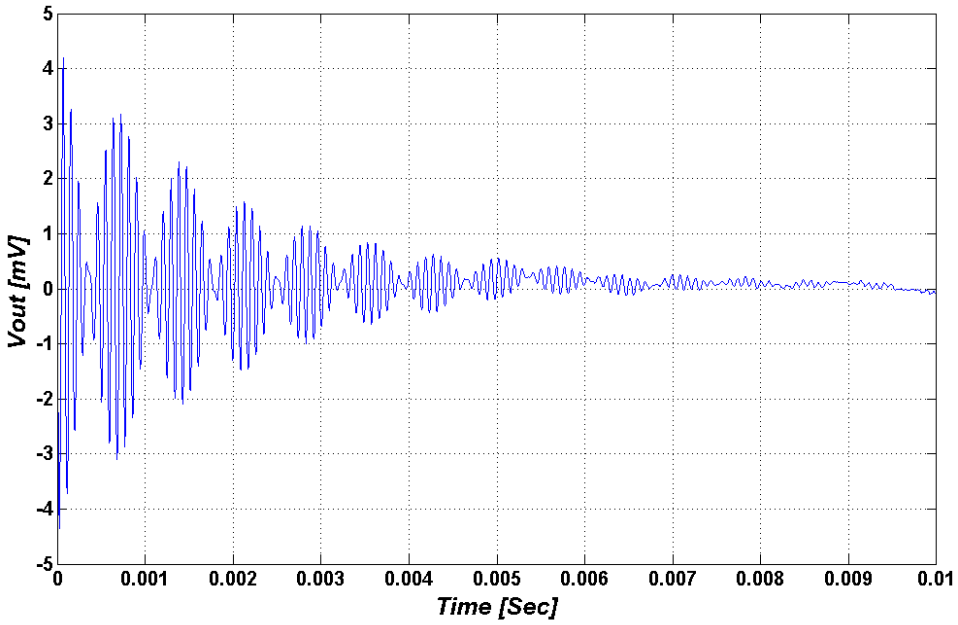

(b)

Fig. 2.8 Simulated NMR spectrum: Simulated NMR signal of (a) Water and (b) Toluene in time domain.

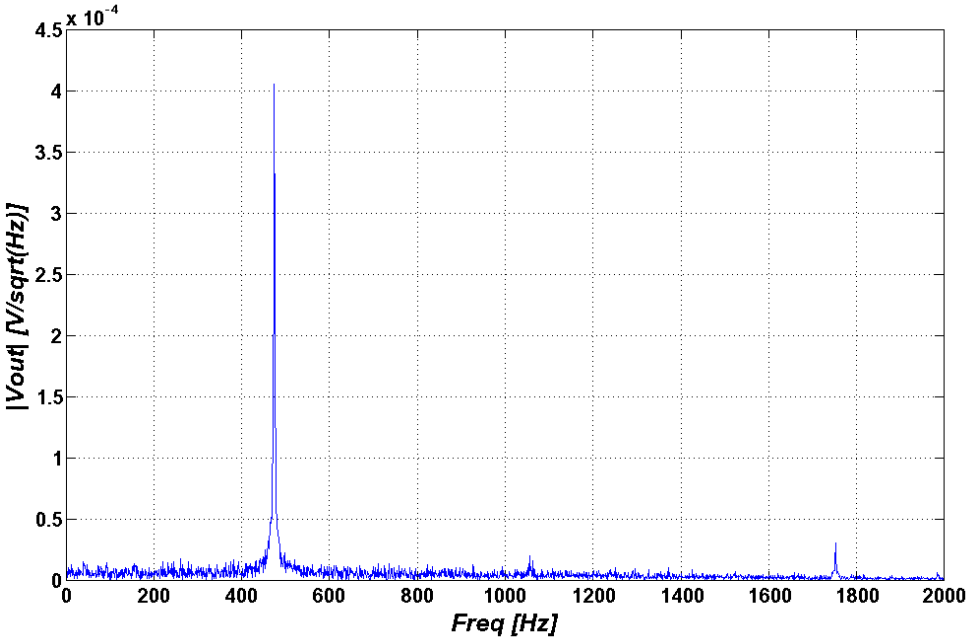

(a)

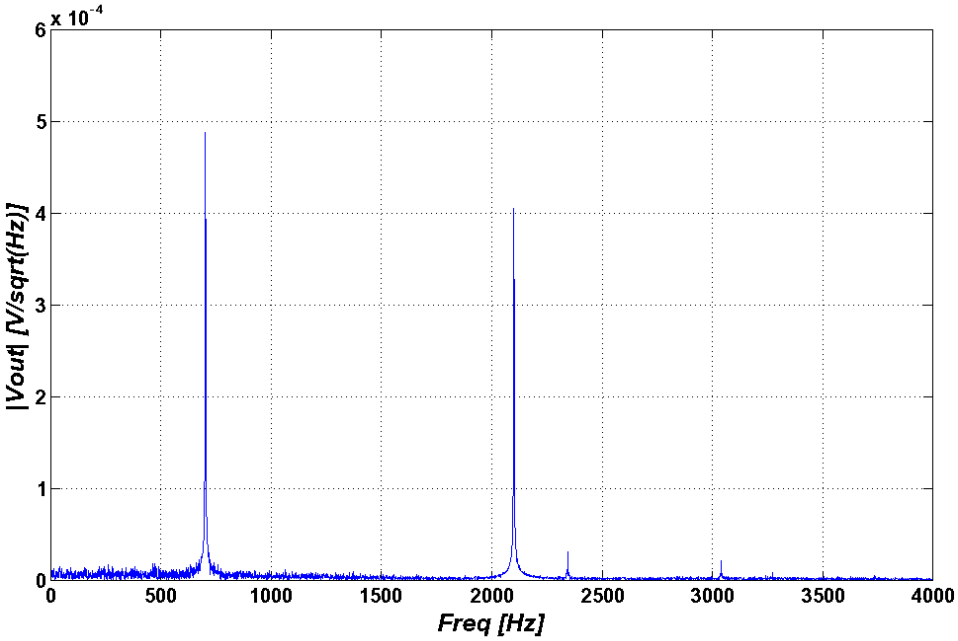

(b)

Fig. 2.9 Simulated NMR spectrum: Simulated NMR signal of (a) Water and (b) Toluene frequency domain.

2.5 Future Work

The development of a micro-hole inside CMOS based on the vertical coils is the key development toward achieving active NMR probes for drug discovery applications. Throughout the current chapter, we have already discussed the vertical µCoil and LNA and presently address this key post-processing factor. Indeed the functionality of a vertical coil in NMR depends on the fact that the sample is placed inside the coil. For this, the creation of micro-holes is a crucial feature in this technique. The chip should also employ a microfluidics structure in order to introduce the chemical samples to the NMR sensors.

The creation of micro-scale through-CMOS holes at the center of the vertical µCoils will be a technological leap that will bring developers closer to the realization of disposable µF devices and reusable CMOS 2D-NMR systems. As described by Uddin *et al*, electron-beam (e-beam) lithography can efficiently be used to drill tiny holes (diameter < 10nm) in a membrane created above the CMOS chip [63]. The creation of such a membrane above the CMOS chip using post-CMOS µfabrication processes is a key step towards the development of various Micro-Electro-Mechanical-Systems (MEMS) like; micro-channels, micro-hot-plates and micro-cantilevers as reported in the literature [64]-[67]. Deep Reactive Ion Etching (DRIE) is also an important post-CMOS processing technique that can accurately back-etch silicon wafers of integrated chips and could also be used for the creation of through-CMOS micro-holes using photolithography masking techniques. However we can study the possibility of using e-beam and Focused Ion Beam (FIB) etching

techniques to increase the precision of the hole-drilling process. It is noteworthy that e-beam and other etching techniques based on ionic diffusion into the etched materials like the FIB etching technique, could prove to be inappropriate for drilling through-wafer holes, when these high aspect-ratio channels are in proximity to active devices inside the CMOS chip. The reason for this is the significant charge injection into active zones possibly causing damage to the doped silicon oxide. The challenge herein is to control the etching process, bringing it to a halt when in proximity of active areas below the surface of the CMOS chip in order to preserve the integrity of µE devices. Despite recent progress in creating nano-holes (to be distinguished from through-CMOS holes) on top of CMOS chips, developing an array of such ducts in proximity of integrated sensors and circuitry, still represents a challenging endeavor. One can develop an array of vertical RF µCoils with through-CMOS IC µholes to direct the sample inside the µCoils using µF structures.

2.6 Conclusion

In this chapter, we put forward the emerging NMR technologies, brief review the challenges and discuss design strategies. µCoils associated with RF interface circuitries were designed and simulated as the core part of the NMR system. We presented a fully integrated CMOS multi-turn differential stacked detection coil and front-end receiver for NMR applications. We also employed a LC resonator as a pre-amplification stage and followed it by a suitable LNA optimized for low input referred noise in order to suitably process the weak NMR signal. The multi-turn differential stacked inductor is integrated on

the CMOS chip with the LNA. The desired on-chip detection inductor is implemented by using 8 layers of the 0.13-μm CMOS technology. Using all 8 layers of the technology allows us to reduce the size of the inductor at a specific frequency. Furthermore, the differential topology of the stacked inductor improves its quality factor without changing the fabrication process. Based on these discussions, we have attempted to convey the multidisciplinary approach needed to active sufficient active NMR probes toward the development of emerging NMR technology for accelerating drug discovery research in the pharmaceutical industry.

Chapter 3
21MHz Dual Path NMR Probe

This chapter lays forward the design and implementation of a fully differential CMOS chip design for low frequency NMR spectroscopy using low magnetic field magnets. Fig. 3.1 Illustrates the new differential technique in comparison with conventional NMR system with a single coil and the proposed differential NMR system using two exciting and two recording millimetre scale coils (mini-coils). The small tubes containing biological or chemical samples are enclosed by mini-coils. One tube is empty and another one is filled with sample. As shown in this figure, the NMR signals of both tubes are detected in order to remove the effect of background NMR signal resulting from the materials of identical sample holders and other devices close sensing sites. The recorded signals are detected using the proposed CMOS circuitry discussed in the following sections.

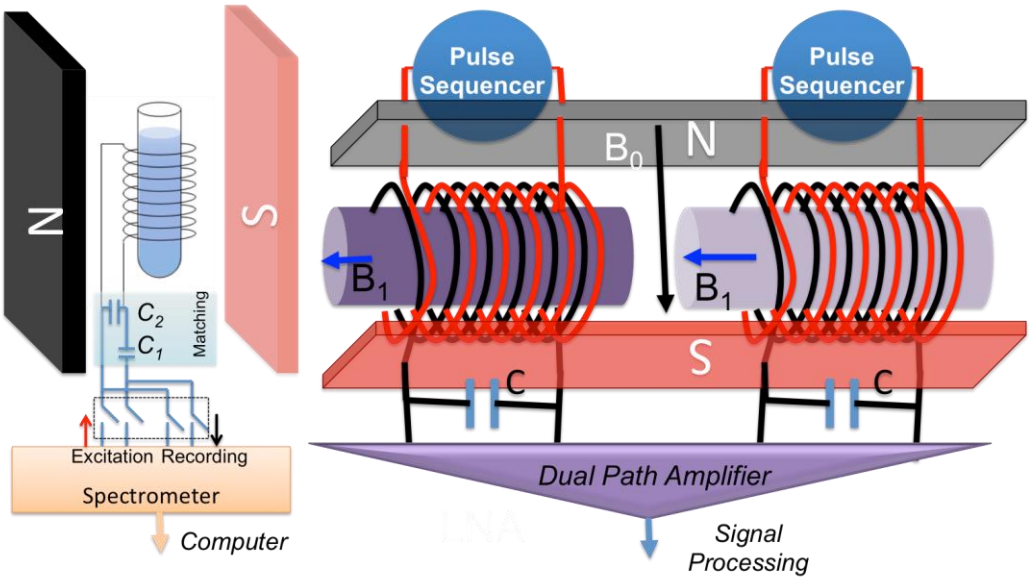

Fig. 3.1 NMR system(a) Convrntional and (b) active NMR probe consisting of Dual-path NMR receiver two pairs of coils.

3.1 Design Methodology

In this section we propose a novel differential system that is connected to two mini-coils for NMR spectroscopy purposes.

3.1.1 Proposed Circuit and System

The proposed receiver (see Fig. 3.2) consists of two off-chip mini-coils connected to a CMOS IC. Off-chip pulse generators are also employed to excite the nuclei within the sample. In this work by knowing that the background noise generated in both sample holders and coils can be subtracted through the differential circuitry, our main focus will be on the transceiver mini-coils and CMOS IC design.

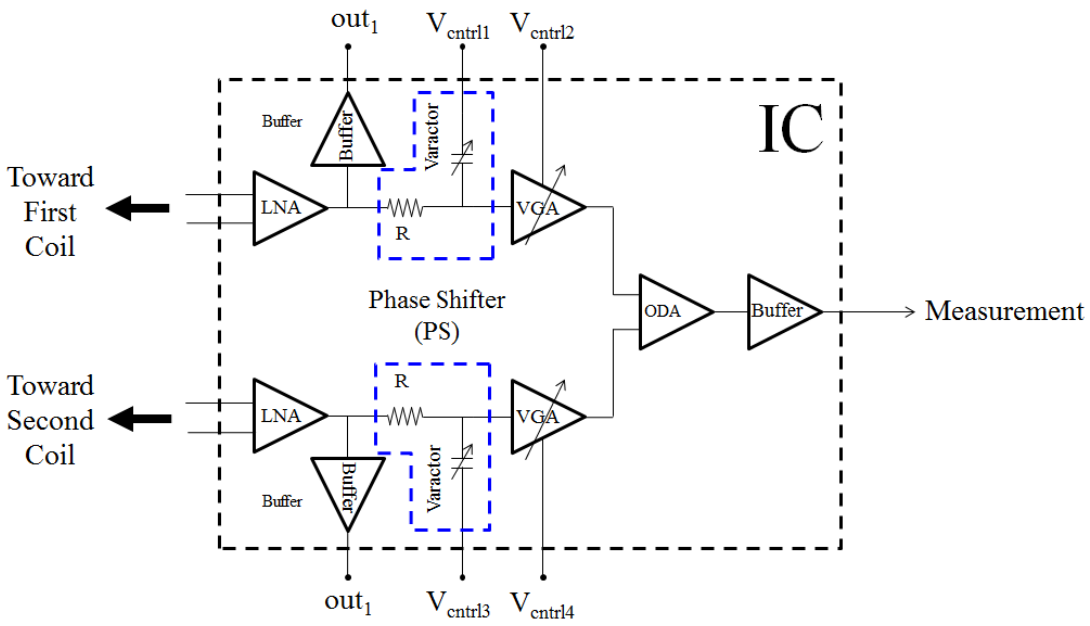

Fig. 3.2 Schematic of proposed doual path NMR receiver (black color) along with off-chip pulse sequencers for RF exciation purposes.

3.1.1.1 IC Design

As seen in Fig. 3.2, the proposed IC includes LNA, phase shifter (PS), variable gain amplifier (VGA), output differential amplifier (ODA) and buffer that will be discussed in the following sub-section.

LNA ($M_{1\text{-}8}$)*:* this is the core part of this design, shown in Fig. 3.3a. A fully differential cascode push-pull LNA is adapted from [38] in order to achieve higher gain and lower noise. Assuming M_1 (M_3) and M_2 (M_4) are identical, the voltage gain of this amplifier is approximately $(g_{m1}+g_{m3}).r_{o8}$, where g_{m1}, g_{m3} are the transconductances of M_1 and M_3 and r_{o8} is the output resistance of M_8. On the other hand, the main sources of current noise in

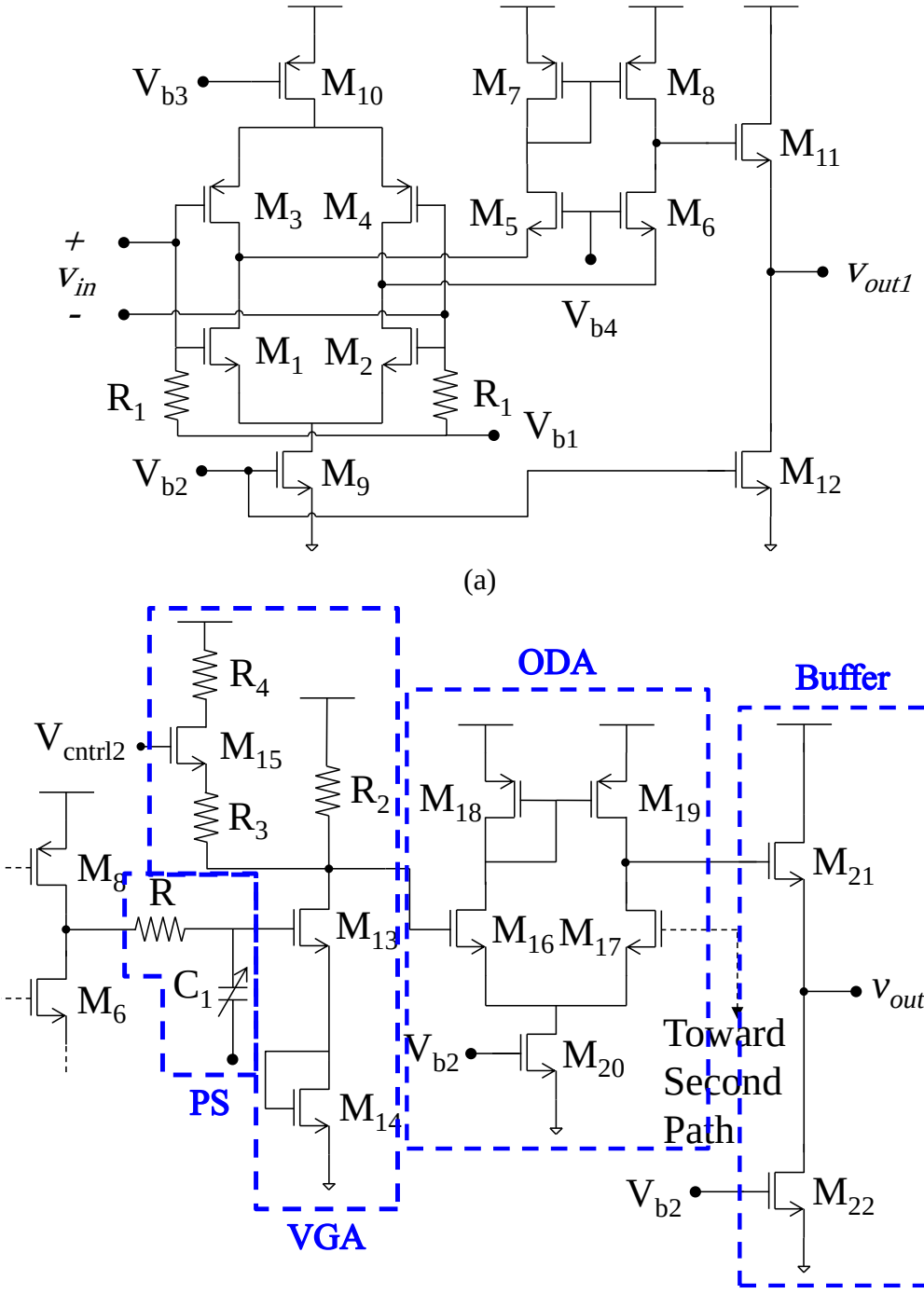

Fig. 3.3 Scehamatic of integrated circuits of (a) LNA, (b) PS, VGA and ODA. A single path 1 is shown in this figure. The second path is connected to ODA.

the circuit are $M_{1\text{-}4}$ and M_8 and the input referred voltage thermal noise, is expressed in EQ. 13

$$\overline{v_{n,in}^{\,2}} = 4kT\gamma\left(\frac{2}{g_{m1}+g_{m3}} + \frac{g_{m8}}{\left(g_{m1}+g_{m3}\right)^2}\right) \tag{13}$$

Where γ is the noise coefficient and g_{m8} is the transconductance of M_8, Based on this equation, a higher DC current can decrease thermal noise, however the self-heating due to the higher power consumption should also be taken into account. It is noteworthy that flicker noise should be added to EQ. 13 especially for low frequency NMR applications.

PS (R, C_v): this is a very critical part of this design needed to remove phase mismatch errors. These errors occur because of the difference between two components. For instance, off-chip mini-coils and LNAs. R and C_v are implemented in CMOS technology using an optional metal layer and on-chip varactor respectively. The PS is adjusted by an external voltage V_{cntrl1}. Thanks to the high impedance of M_{13}, the gain and the phase shift of this phase shifter are $1/(1+RC_1\omega^2)$ and $-\tan^{-1}(RC_1\omega^2)$ respectively.

VGA ($M_{13\text{-}15}$, R_2, R_3 and R_4) is designed to adjust the level of the output signal in the linear zone using the external voltage control V_{cntrl2}. This signal is varied due to the input NMR signal changes. By assuming $G = g_{m13}g_{m14}/(g_{m13}+g_{m14})$ and $R_2 >> (R_3 + R_4)$, the voltage gain of the VGA varies between GR_2 and $G(R_3+R_4)$.

ODA ($M_{16\text{-}19}$): is designed to differentiate the signals generated in two different signal paths. The gain of this stage is $g_{m16}.r_{o19}$ where g_{m16} is the transconductance of M_{16} and r_{o19} is the output resistance of M_{19}. All PS, VGA, and ODA are shown in Fig. 3.3.

3.1.1.2 Mini-Coil and Passive Amplifier

As described in section 2.1, the development of the low frequency on-chip coil for NMR spectroscopy results in a very low quality factor (Q) coil and occupies a large area. For this reason, we have developed a low complexity solenoid mini-coil as shown in Fig. 3.4. In this figure the HFSS model and the equivalent circuit, including the parasitic resistance and capacitance between the wires, is drawn. In this mini-coil design, the strength and uniformity of the magnetic field B_1 are the key parameters to be maximized as demonstrated and discussed in next section. Another important factor in this design is the selection of capacitor C in parallel with the mini-coil in order to boost the signal according to the voltage gain of the LC resonator ($|A_{v\text{-}LC}| = 1/\sqrt{((1-R_S C\omega Q_L)^2+(R_S C\omega)^2}$). In this equation, the Q_L ($L\omega/R_S$) is the quality factor of the mini-coil with inductance L and resistance R_S. The derivative of this equation at C can be used to search for the capacitance setting that maximizes the gain of LC circuit. This capacitor is obtained to be ($C_{max} = Q_L/R_S C(1+Q_L^2)$) and its voltage gain is $\sqrt{(1+Q_L^2}$).

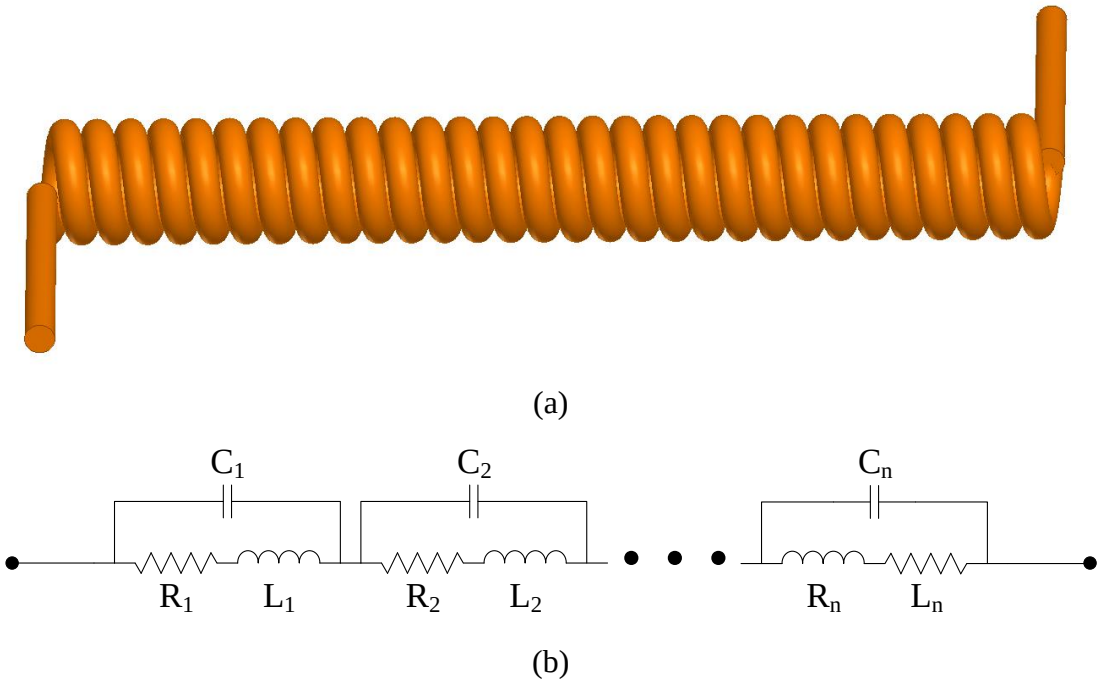

Fig. 3.4 Mini-coil models: (a) HFSS Model and (b) its equivalent circuit

3.2 Results

In this section, we demonstrate and discuss the Cadence Spectre simulation results of the CMOS chip, the finite-element ANSYS HFSS simulation results of the mini-coil, and the experimental results.

3.2.1 Fabrication Results and Setup

The IC described in section 3.1.1.1, was fabricated using a 0.13-µm IBM CMOS process. The layout of this chip is shown in Fig. 3.5a.

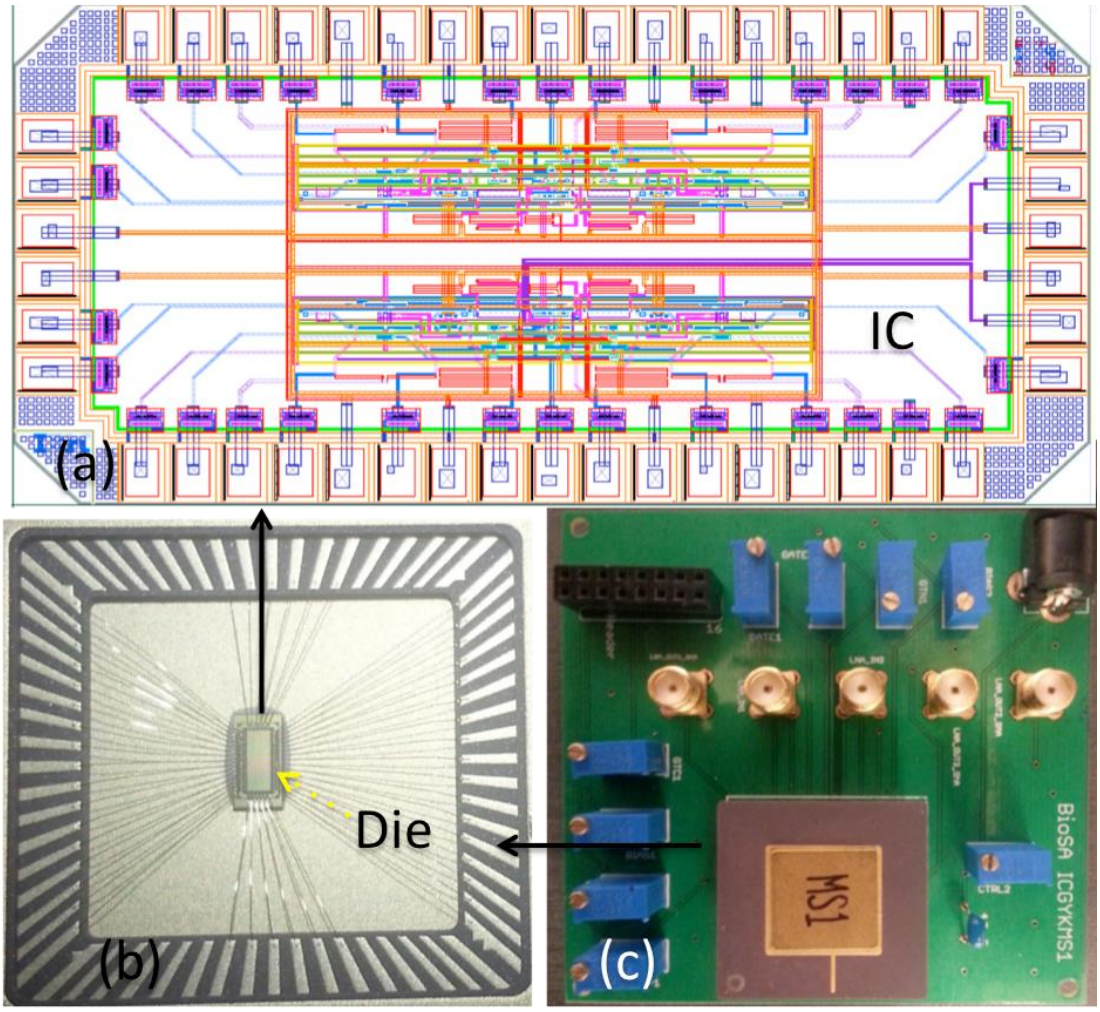

Fig. 3.5 Fabrication Results: (a) Layout of IC including LNAs, VGAs, PSs, ODAs and buffers's building blocks, (b) packged chip including CMOS fabricated die wirebonded to the package and (c) PCB including discreet devices and the packaged chip.

The fabricated chip was bonded on a Ceramic Package (CPG06820) (Fig. 3.5b). Thereafter, the package was assembled on a printed circuit board (PCB). This PCB was fabricated for test and characterization of the CMOS chip (see Fig. 3.5c).

The test setup consists of a power supply voltage, RF signal generator, oscilloscope, and vector network analyzer (VNA) as seen in Fig. 3.6a. Another important part of the measurement setup is the static magnet. In this work, we use a pair of small cubic NdFeB permanent magnets. The mini-coil, prepared using copper wires (see Fig. 3.6b) surrounding a glass tube, is placed in between these two magnets.

3.2.2 IC Simulations

LNA: As already mentioned two important parameters in our proposed IC are the voltage gain and noise performance. The voltage gain of the LNA vs frequency in different corners of the process is shown in Fig. 3.7a. In the worst case, the low voltage gain due to the process variation can be compensated using the VGA. Also, the noise performance of the LNA vs frequency in different corners of the process is shown in Fig. 3.7b. Based on these results, the LNA has been designed successfully for NMR applications.

PS: Another important parameter in the proposed differential receiver is the dynamic range of the phase shifter. In this design, the range of the phase is around 5 degrees while the voltage gain is almost constant in this range as seen in Fig. 3.8.

VGA: Herein we also simulated the range of gain variation in order to prove the functionality of the VGA. The range of the voltage gain vs control voltage is shown in Fig. 3.9. Based on this result the gain can be doubled by changing the V_{cntrl} from 900 to 1075 mV.

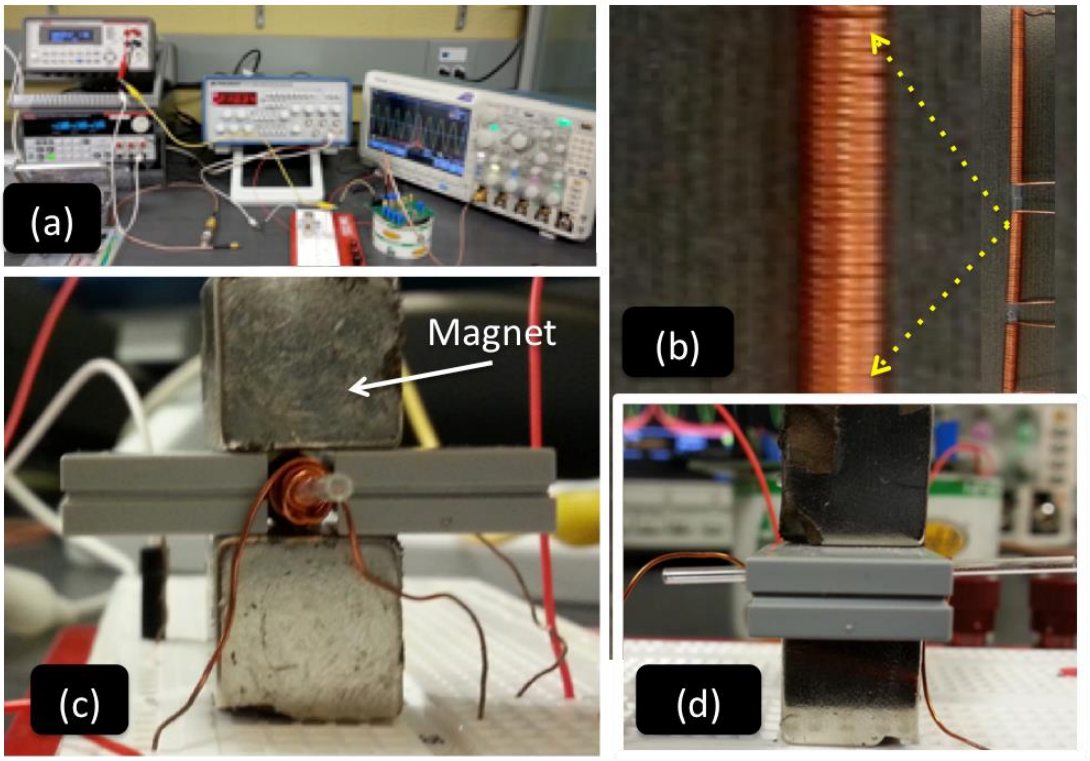

Fig. 3.6 Multidisciplinary Measurement Setup: photographs of (a) the electrical characterizations' tools, (b) mini-Coils along with a zoom-in's photo, (c) the static magents in the bottom and top of mini-Coil suronunding smaple holder's glass mini-tube and (d) the same image of magents from different agngle.

ODA: The last stage in the proposed IC is a differential amplifier that measures the difference between the signals received from two paths. By considering the NMR background signal generated by the material of a sample holder, we modeled these signals as shown in Fig. 3.10a and Fig. 3.10b. The output signal of the receiver shown in Fig. 3.10c does not include the background signal at 20MHz. The details of this procedure will describe in the following spectral analysis section.

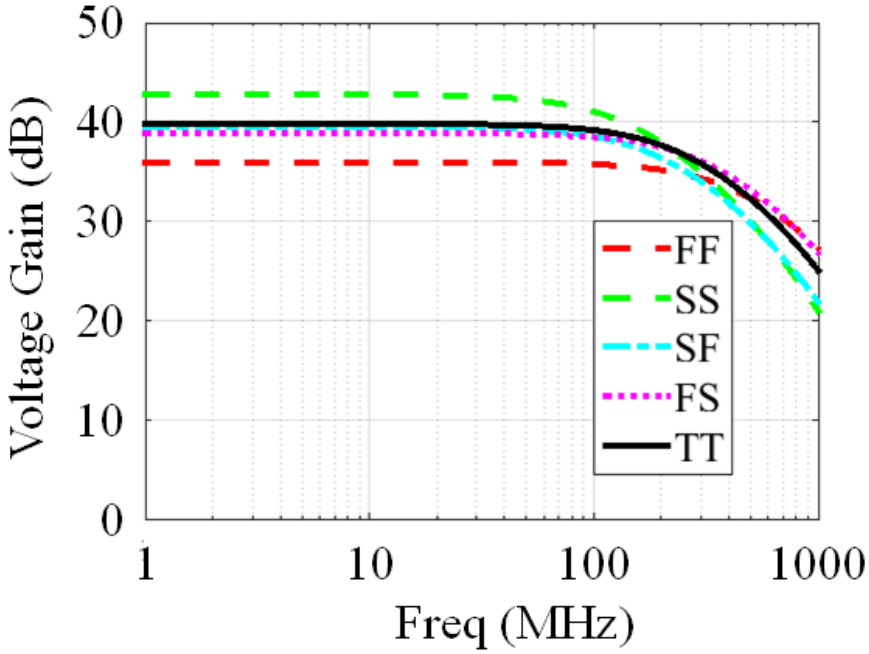

(a)

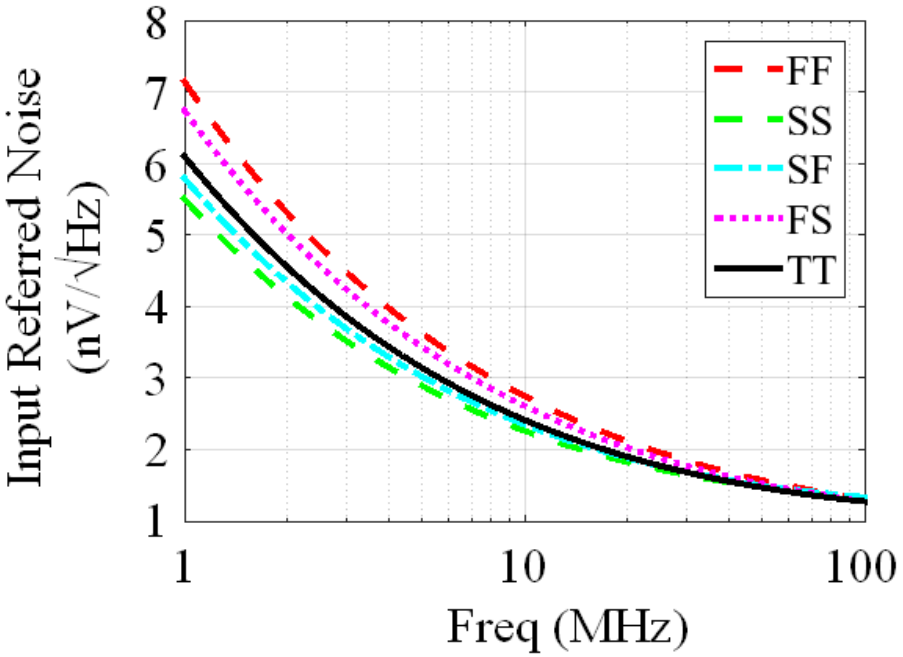

(b)

Fig. 3.7 Cadance Simulation Results: (a) Voltagr Gain and (b) Noise performance in five different corners.

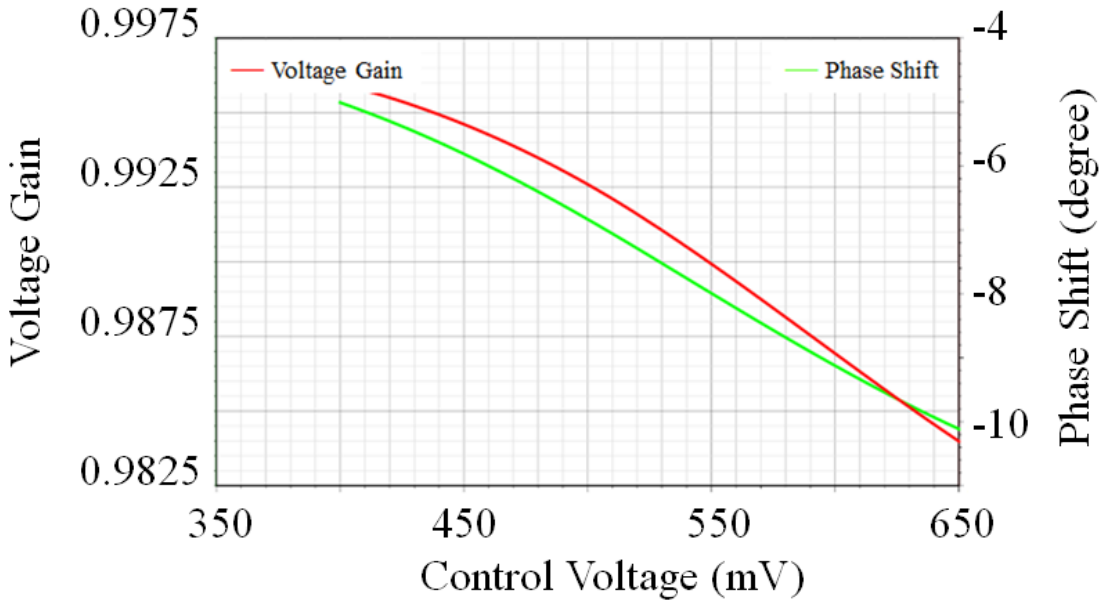

Fig. 3.8 PS simulation results while the voltage gain is almost constant

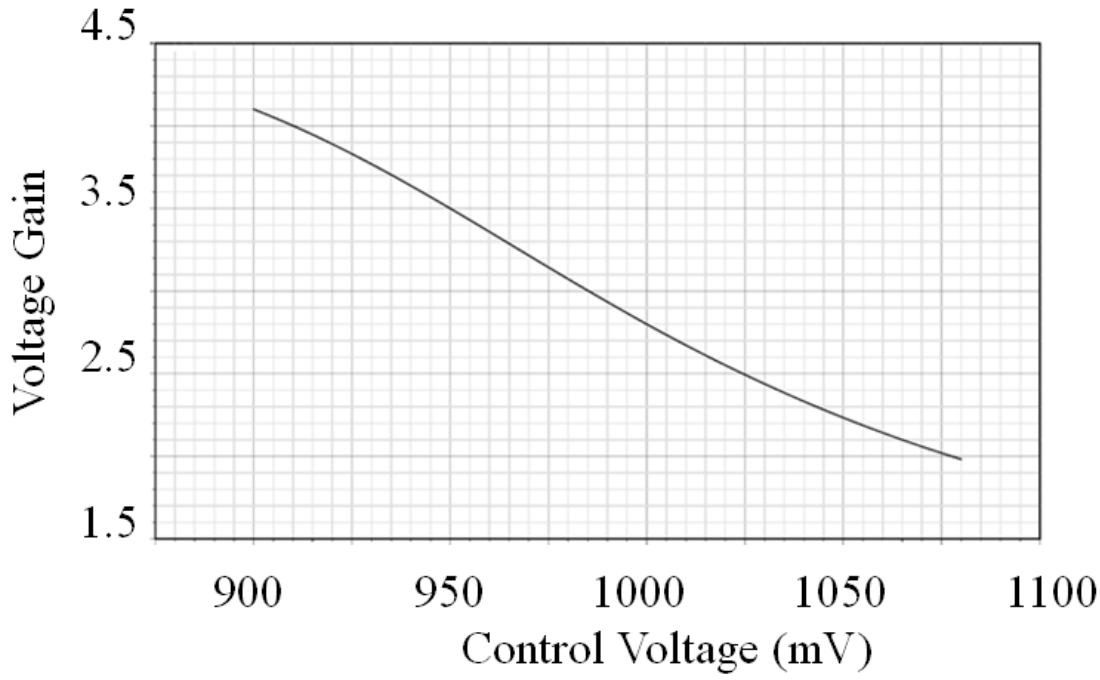

Fig. 3.9 VGA simulation results as function of voltage control

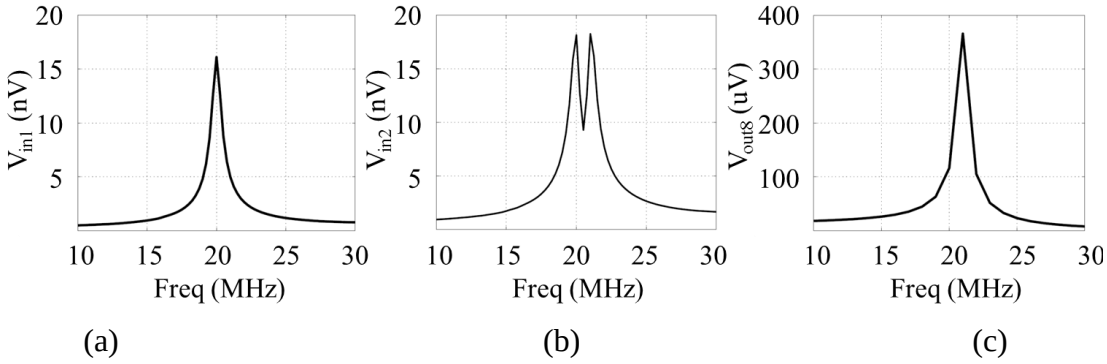

Fig. 3.10 Dual-path reciever simulation: NMR signal(s) associated with (a) target chemical molecoules (e.g. water), (b) other mateials (e.g. sample holder) and (c) the output of reciever after amplification.

Spectral Analysis: As already mentioned, the proposed dual path receiver offers the advantages of removing the NMR background signals. Herein the functionality of the receiver in this regard is demonstrated by observing the appropriate frequency shift of different chemical materials. In the simulation, we have assumed that the background signal with one fundamental frequency at 20 MHz is applied to one path of the receiver (see Fig. 3.10a) and the NMR signal along with background signal with two frequencies at 21 MHz and 20 MHz are applied to the another path (see Fig. 3.10b). The output signal of the receiver (see Fig. 3.10c) successfully shows the removal of the 20MHz signal associated with the microfluidics sample holder. Some characteristics of the designed CMOS chip are summarized in Table 3.

Furthermore, the NMR signals associated with water and toluene are modeled and included in the simulations. The frequency shift of water at 21 MHz is about 88 Hz from 21 MHz

Table 3: CMOS Chip Specifications

Technology	CMOS 0.13µm
Area (mm^2)	1×2
Vdd [V]	1.6
DC current of the LNA core [mA]	3.4
LNA 3-dB BW [MHz]	800
Operation Frequency [MHz]	21
Voltage Gain [dB] @ 300MHz	42.85
Varactor resolution (fF/mV)	1.6
Phase shift range (degree)	5
VGA range (dB)	6

as shown in Fig. 3.11a and Fig. 3.11b. Also, the frequency shift of the toluene at 21 MHz should be 40 Hz and 138 Hz from 21 MHz as shown in Fig. 3.11c and Fig. 3.11d.

3.2.3 Mini-Coil Simulations and Characterization

Simulations: A MW35C magnet wire was used to fabricate the mini-coils. The diameter of this wire is 404 µm, the inner diameter of the solenoid is around 1mm and the pitch between wires is about 500 µm. The ANSYS HFSS simulator is used to model and simulate three coils with 35, 50 and 100 turns. The magnetic fields B_1 in the *xy*-plane and the *z* direction are demonstrated in Fig. 3.12a and Fig. 3.12b. These simulations verify the uniformity of the magnetic field B_1 in the z direction and the near absence of magnetic field in the *x* and *y* directions. The inductance and quality factor simulation results are also shown in Fig. 3.12c and Fig. 3.12d. As our desired frequency should be around 21

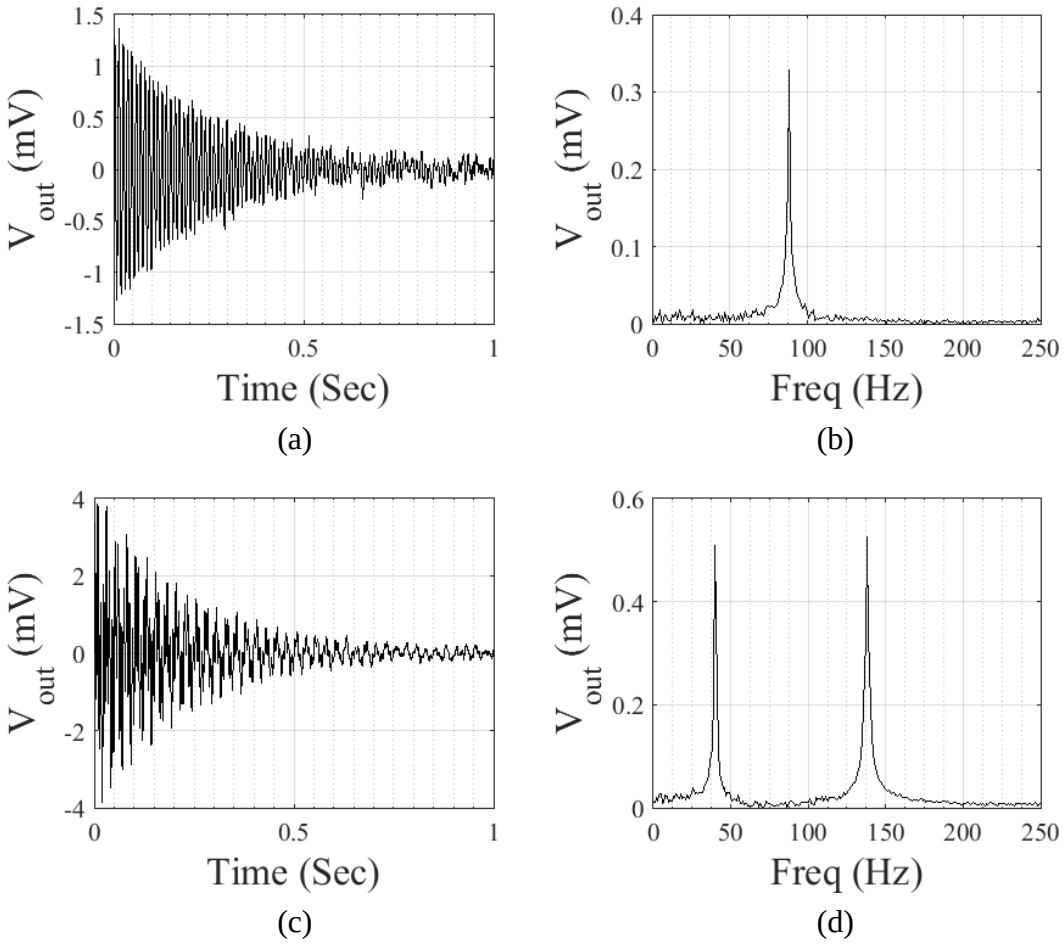

Fig. 3.11 NMR signal simulation results of (a), (b) Water, and (c), (d) Toluene in time and frequency domains respectively.

MHz, according to the simulation results the mini-coil should have around 100 turns. The operational frequency of the coil is equal to the frequency at the peak of the quality factor.

Characterization: Three different mini-coils with varying turn numbers (N = 35, 50, 100) were prepared. These coils were characterized using a VNA and the real- and

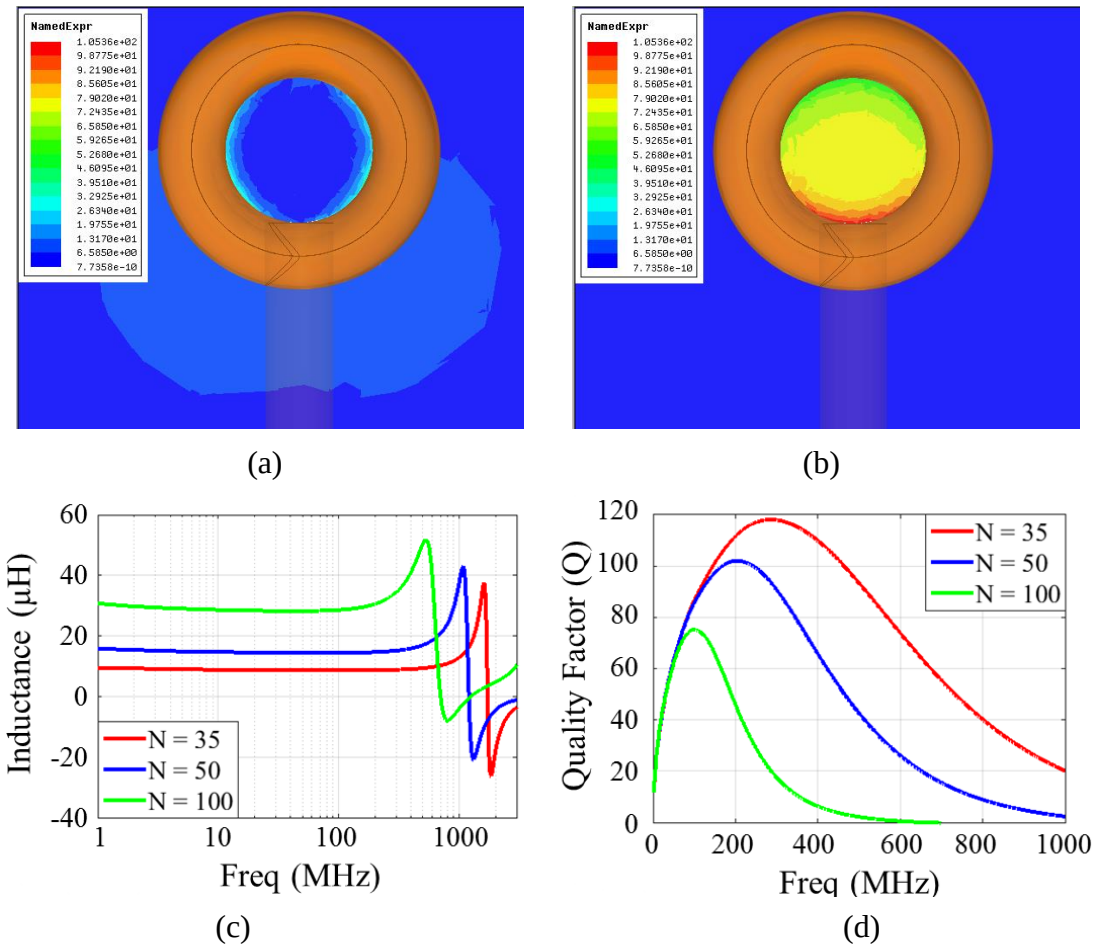

Fig. 3.12 HFSS Simulation results: (a) B_1 in *xy*-plane (b) B_1 in *z*-directio (c) inductance vs frequency, and (d) qulity factor vs frequency

imaginary components of S_{11} for the three mini-coils were extracted; these results are shown in Fig. 3.13a and Fig. 3.13b. Also, the inductance and the quality factor of the coils were characterized and are shown in Fig. 3.13c, Fig. 3.13d, respectively. As apparent in Fig. 3.13d, the solenoid mini-coil with around 100 turns has a lower operational frequency and is the best option for the 21 MHz NMR.

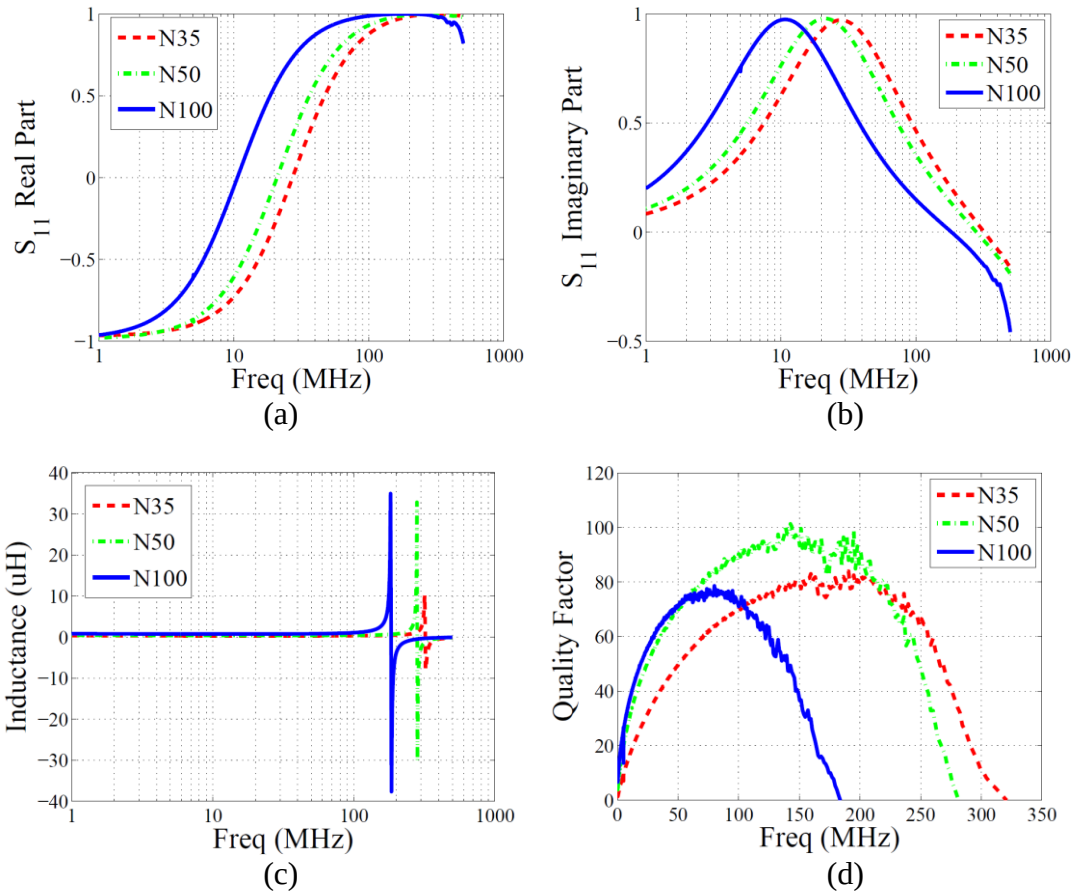

Fig. 3.13 Characterization results of mini-Coil: (a) real part of S_{11} and (b) imaginary part of S_{11} (c) inductance and (d) quality factor as a function of frequency.

3.2.4 Experimental Results

The chip was characterized using various test configurations including single path #1, single path #2 and dual paths as shown in Fig. 3.14. A low complexity setup has been developed using two coils in the form of an RF transformer. A variable amplitude signal can be generated using this setup for the characterization of our device. The input and

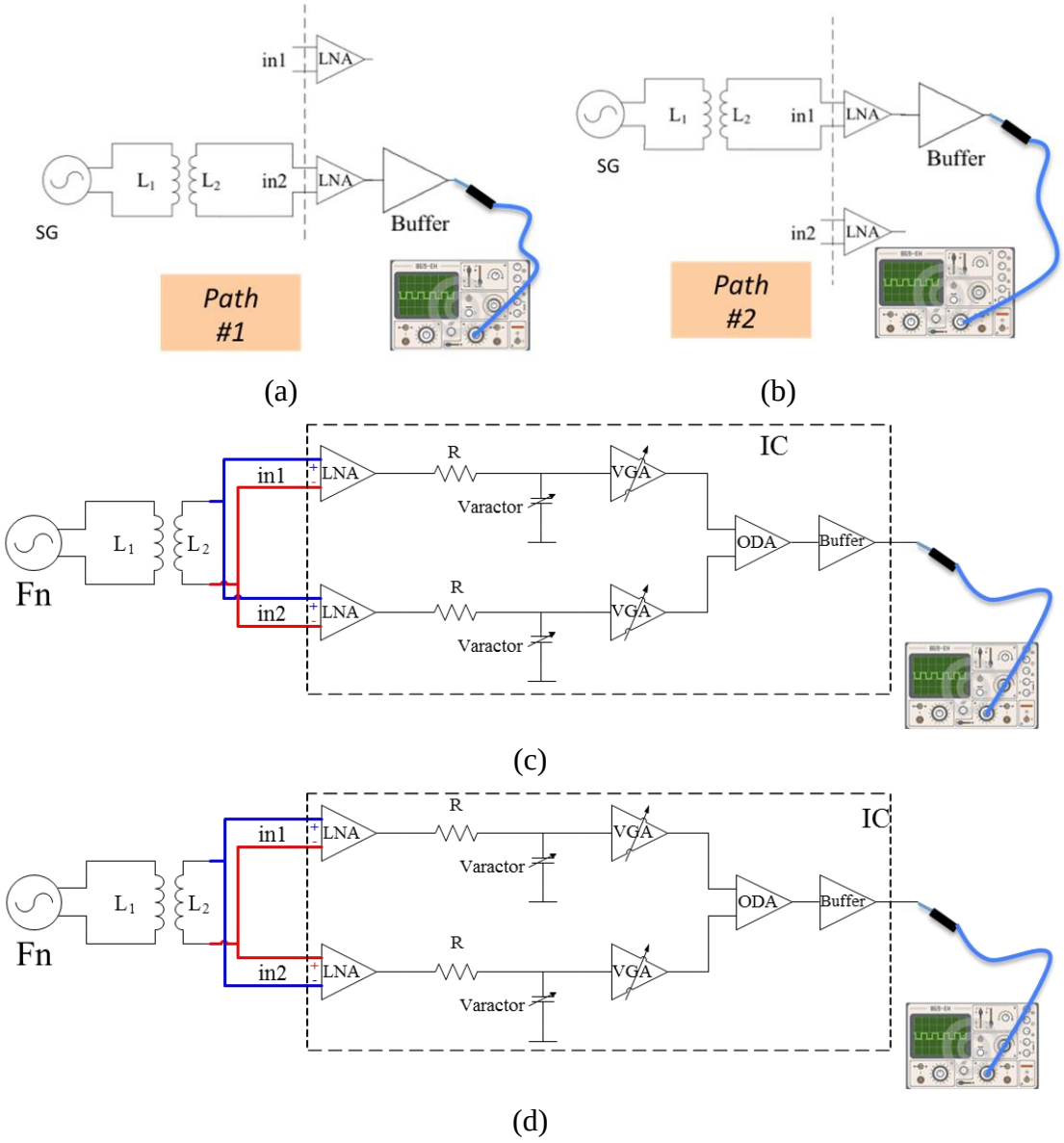

Fig. 3.14 Masurement scenarios including single (a) path 1, (b) single path 2 and dual-path (c) in-phase and (d) out-of-phase

output signals of the LNAs along with the excitation signal were measured separately as seen in Fig. 3.15a and Fig. 3.15b. As demonstrated in these figures, the gains of both

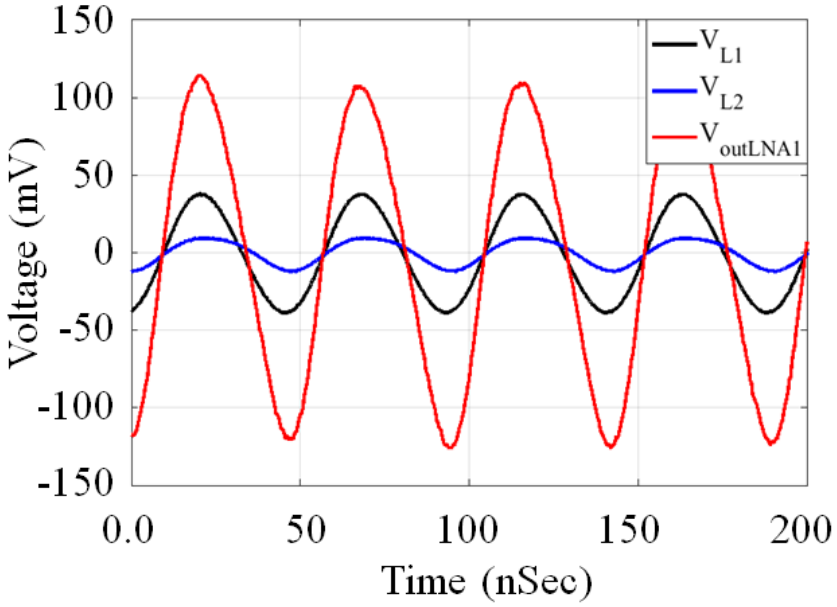

(a)

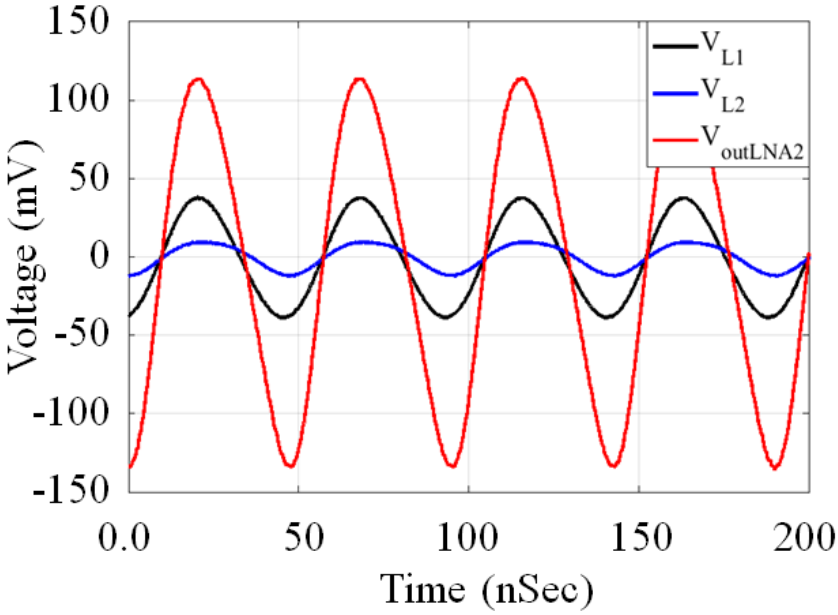

(b)

Fig. 3.15 Single path measurement: (a) path 1, (b) path 2. In these measurement results, three signal of input, outputs are shown.

LNAs are about 24 dB. The simulation results show higher values because the bias currents and voltages are different from the ones in practice.

The adjustment of DC bias using high precision power supplies can result in higher gain in our measurements. The dual path receiver's voltage gain was measured using in-phase measurement modes as seen in Fig. 3.16. In order to prove the functionality of the system in cancelling the undesired background frequency, the characterization in differential modes is very crucial. For this we measured the voltage at the input and output of the receiver as shown in Fig. 3.16a and Fig. 3.16b, respectively. As seen therein the signal of the input at 21 MHz is attenuated at the output of the differential receiver, in the in-phase mode, and it has been amplified in the out-of-phase modes (see Fig. 3.16c). Based on these characterizations, we successfully demonstrated the functionality of the chip and this design can be used in the future for the development of fully integrated NMR.

3.3 Discussions

In this section we discuss some of the practical issues associated with the design and implementation of low cost NMR spectroscopy tool. CMOS technology, by offering a low cost platform and multiple metal layers, is the best candidate to design three (3D) dimensional μCoils with specific geometry suitable for high SNR NMR spectroscopy. Herein, first we discuss the advantages and disadvantages of using on-chip μCoils for

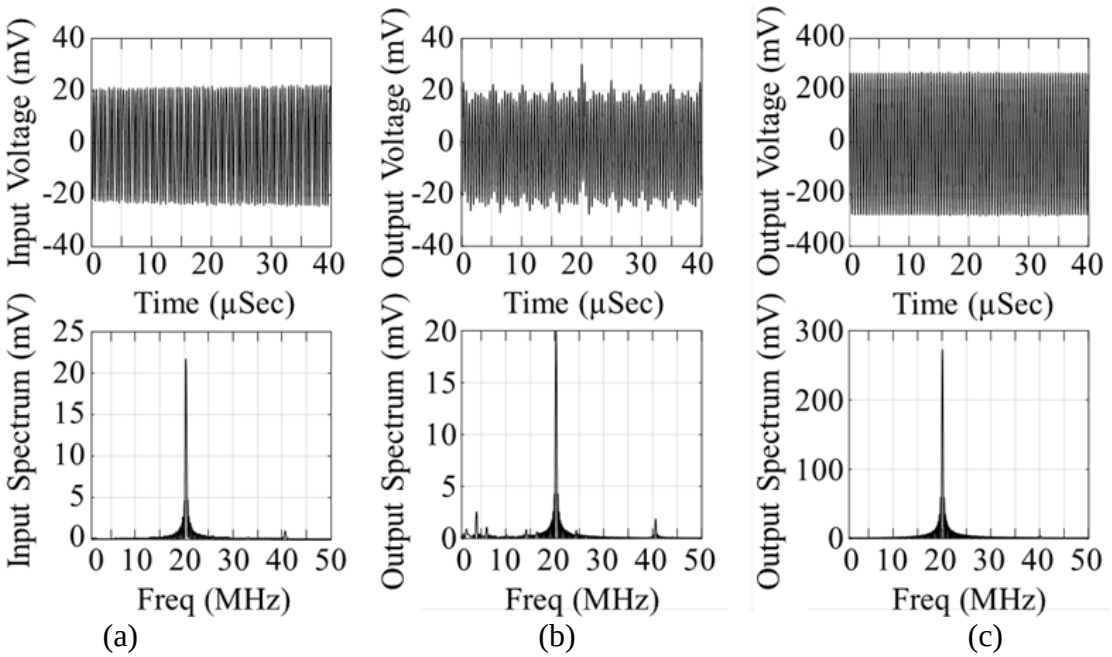

(a) (b) (c)

Fig. 3.16 Spectral measurement results: (a) Input voltage of the receiver in time domain and frequency domain (b) output voltage of the receiver in in-phase mode in time domain and frequency domain (c) output voltage of the receiver in out-of-phase mode in time domain and frequency domain.

low cost NMR spectroscopy and then we mention other issues and future works in this approach.

3.3.1 Integrated μCoil

CMOS technology is the best candidate to design the μCoils using multilayers of metals. For this reason, we designed an eight-layer solenoid on chip as shown in Fig. 3.17a. Due to the parasitic capacitance and resistances generated between the layers and between the circular coils in each layer (see Fig. 3.17b), the quality factor of such a μCoil at low

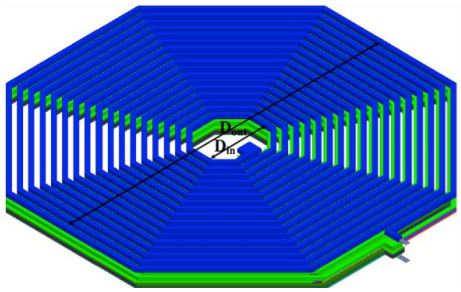

(a)

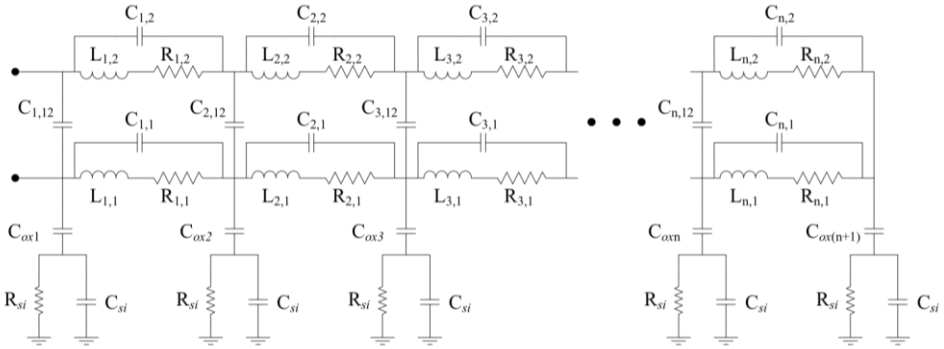

(b)

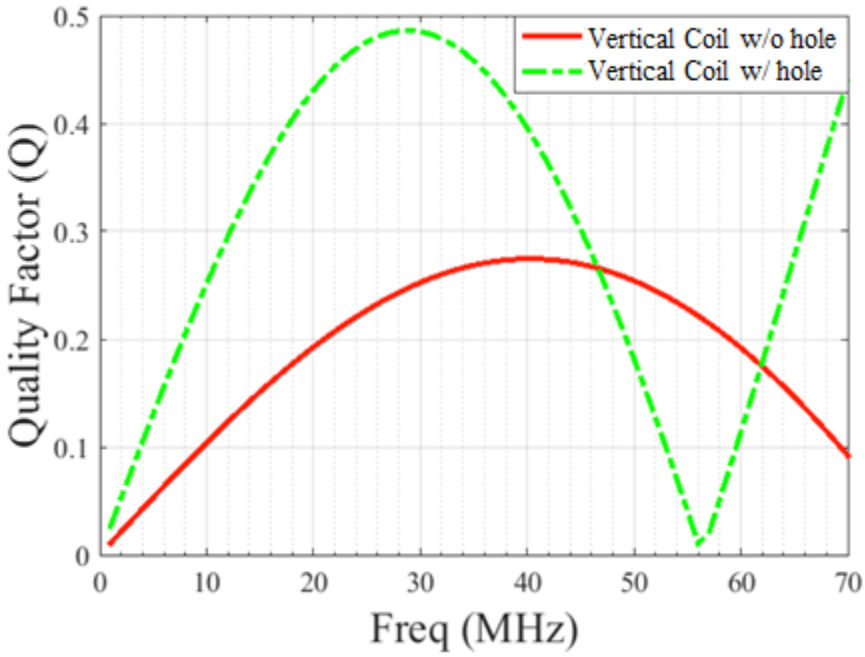

(c)

Fig. 3.17 On-chip solenoid on-chip (a) 3D CMOS μCoil, (c) equivalent circuit and (d) quality factor with/without hole inside.

frequencies is low. Specifically, as seen in Fig. 3.17c, the quality factor of this CMOS-based coil is around 0.25. By creating the hole in the center of the coil, the quality factor is slightly improved; however, in the presence of the sample the quality factor can be lower than this value. The quality factor can slightly vary by changing the sample. Therefore, based on this result, for our 20-MHz design discussed in this thesis, we used a mini-coil instead of integrated µCoil.

3.3.2 Other Practical Issues

Among various practical issues associated with the proposed low cost NMR spectroscopy tool, microfluidics and shielding topics are briefly discussed.

Microfluidics: The miniaturized NMR system devices include µ- or mini-coils surrounding the sample. Therefore, micro-channels should be incorporated in directing such small samples toward the sensing sites in NMR systems incorporating coil technology of this kind. Such µL/nL samples should be placed in the center of the uniform magnetic field B_1 using microfluidics with NMR compatible materials. This is because the generated NMR signal by the sample holder should be minimized. By using the microfabrication technology, the design and implementation of microfluidics structures is feasible. However, in this thesis, we discussed how the differential dual path could offer a solution to overcome this problem by removing the magnetic background interference arising in such situations.

Electromagnetic Compatibility is an important issue in magnetic sensing systems. As the core of NMR spectroscopy is the excitation and recording of an RF signal, the separation of an actual NMR signal from other electromagnetic interferences is a challenge. In other words, to prevent the electromagnetic interferences from reaching the sensing sites of an NMR system, an appropriate shielding package should be prepared. This package should include an opening for sample delivery and readings using photolithography techniques.

3.3.3 Future Works

In this thesis, we presented and discussed a new research approach called low cost NMR spectroscopy. As a first step, we discussed the design and implementation of a critical part of this design, which is the dual path receiver. In the simulation and experimental platform, the signals were measured in the presence of magnetic chemical solutions in order to expose the active probe to actual test conditions. However, these results cannot show the functionality of the proposed circuit for NMR spectroscopy. As already mentioned, it is important to design a new chip and fully electrical and NMR characterization should be performed.

The current work discussed in this chapter will be advanced by accurately characterizing the magnetic field of low-strength magnet and also expanded through the study of the effects of non-uniformity of static magnet fields on the quality of NMR spectroscopy. Thereafter the complete spectrometer (combined analog and digital signal processing) should be designed and implemented in order to extract the NMR signal and compare it

with other standard techniques. A major step toward NMR PoC diagnostics is to study the relation between the NMR signals and harmful cells/biomolecules by incorporating the active NMR probe, magnet and microfluidic structure for low cost NMR spectroscopy purposes.

3.3.4 Summary

In this chapter, we proposed a new approach for developing a low cost NMR system. As a first step of this approach, we described the design and implementation of a fully integrated CMOS dual-path receiver for NMR applications. This dual-path receiver is implemented in a 0.13-µm CMOS technology. Cadence and ANSYS HFSS were used to simulate the integrated circuit and mini-coil. Furthermore, the experimental characterizations of the chip were also performed using a low complexity setup including a cheap magnet and a mini-coil surrounding a glass tube. The simulation and experimental results verified the functionality of the proposed integrated fully differential dual path amplifier strategy. The proposed device offers an important advantage for NMR spectroscopy.

Chapter 4
Contributions and Future Works

This chapter provides a summary of the proposed techniques and contributions achieved from these research studies. In the research program proposed in the Biologically Inspired Sensors And Actuators Laboratory, the short-term goal is the design and implement integrated circuit designs dedicated to emerging NMR technologies. The long-term goal is to completely implement the NMR system by incorporating the proposed integrated circuits. This thesis has successfully taken the first step toward by proposing new circuit and sensor techniques. In the remaining of this chapter, the main contributions and practical problems are discussed and then briefly the future directions put forward.

4.1 Contributions

The focus of this project was placed on the design, implementation and characterization of CMOS chip for NMR spectroscopy. In this direction, the following research results and contributions were achieved.

1) A novel Three Dimensional (3D) CMOS Based RF µCoil dedicated to NMR spectroscopy was proposed. This new design was verified using the following results.

   a) HFSS Simulation results were demonstrated.

   b) Spectral Analysis were demonstrated.

2) A novel CMOS based dual path receiver for NMR spectroscopy was proposed. This new design was verified using the following results.

   a) Custom made Integrated Circuit design and Implementation using 0.13-µm IBM CMOS

   b) Cadence Simulation results were demonstrated and discussed.

3) First CMOS Chip design, fabricated and characterized in York University

This project describes the first successful effort in the department of electrical engineering and computer science, York University to design and implement a CMOS Integrated circuit

using standard technology. For this reason, the early stage of this research was dedicated to the preparation and adjustment CAD tool and after the simulation and submission of chip the fabrication and test of device was performed successfully.

4) The achieved results were published/submitted in the following list of conference or journal papers:

1) Active nuclear magnetic resonance probe: A new multidiciplinary approach toward highly sensitive biomolecoular spectroscopy, *IEEE International Symposium on Circuits and Systems (ISCAS)*, Lisbon, Portugal, 2015

2) Dual-path NMR Receiver using Double Transceiver Microcoils, *35th Annual International Conference of the IEEE Engineering in Medicine and Biology Society (EMBC)*, Milan, Italy, 2015.

3) Dual Path Nuclear Magnetic ResonanceReceiver: A Multidisciplinary Approach Towards Low Cost Bimolecular Spectroscopy, *IEEE Transactions on Biomedical Circuits and Systems*, Submitted Oct. 5th, 2015 (Invited Paper).

4) Active Nuclear Magnetic Resonance Probe: A New Multidisciplinary Approach Toward Highly Sensitive Biomolecular Spectroscopy, *IEEE Transcations on Circuits and Systems I*, Submitted Oct. 7th, 2015 (Invited Paper).

5) Diffrentail CMOS NMR Spectroscopy: Design and Implementation and Experimental Results, *IEEE International Symposium on Circuits and Systems (ISCAS)*, Montreal, Canada, 2016 (Submitted).

4.2 Future Works

As already mentioned, this master thesis has successfully taken a small step toward an emerging NMR technology. Many efforts should be taken to complete the system for an actual NMR spectroscopy. Among these efforts, the following key steps should be taken to achieve a successful NMR spectroscopy.

1) Fully integrated circuit: In both approaches described in chapter 2 and 3, only the recording system were designed and/or implemented. Therefore, the complete system design should be performed and the new chips are fabricated. The voltage gain and input referred noise can be improved in order to achieve better results. In this thesis, we discuss the required main parameters of CMOS chip for NMR spectroscopy. However, a new fully integrated CMOS chip should be designed and characterized.

2) Post-Processing: The creation of holes in the center of CMOS chip after the chip fabrication is the key step to direct the sample toward the vertical coil. For this, novel method should be developed in order to perform the required post CMOS processing without damaging the underneath circuitry.

3) NMR spectroscopy: After the design and implementation of CMOS chip the NMR spectroscopy is the mandatory step towards the development of new technology. For this reason, it is important to characterize the created magnetic field and assure of uniformity as well as its strength over the sensing site. Based on these characterization results, the

circuit design should accordingly calibrate in terms of operating frequency and voltage gain.

4) Sample Delivery: A major step after the completion of CMOS design and fabrication is to develop microfluidic structures to deliver a small sample towards the sensing site. For this reason, the development of an NMR-compatible microfluidics structure is another challenge in this direction.

References

[1] J. K. Rosenstein, M. Wanunu, C. A. Merchant, M. Drndic, and K. L. Shepard, "Integrated nanopore sensing platform with sub-microsecond temporal resolution," *Nature methods,* vol. 9, pp. 487-492, 2012.

[2] Y. Chen, C. C. Wong, T. S. Pui, R. Nadipalli, R. Weerasekera, J. Chandran, *et al.*, "CMOS high density electrical impedance biosensor array for tumor cell detection," *Sensors and Actuators B: Chemical,* vol. 173, pp. 903-907, 2012.

[3] M. M. Ahmadi and G. A. Jullien, "A wireless-implantable microsystem for continuous blood glucose monitoring," *Biomedical Circuits and Systems, IEEE Transactions on,* vol. 3, pp. 169-180, 2009.

[4] A. Scott, K. Weir, C. Easton, W. Huynh, W. J. Moody, and A. Folch, "A microfluidic microelectrode array for simultaneous electrophysiology, chemical stimulation, and imaging of brain slices," *Lab on a Chip,* vol. 13, pp. 527-535, 2013.

[5] E. Ghafar-Zadeh, M. Sawan, V. P. Chodavarapu, and T. Hosseini-Nia, "Bacteria growth monitoring through a differential CMOS capacitive sensor," *Biomedical Circuits and Systems, IEEE Transactions on,* vol. 4, pp. 232-238, 2010.

[6] H. Eltoukhy, K. Salama, and A. E. Gamal, "A 0.18-μm CMOS bioluminescence detection lab-on-chip," *Solid-State Circuits, IEEE Journal of,* vol. 41, pp. 651-662, 2006.

[7] D. Hall, R. S. Gaster, K. Makinwa, S. X. Wang, and B. Murmann, "A 256 Pixel Magnetoresistive Biosensor Microarray in 0.18 μm CMOS," *Solid-State Circuits, IEEE Journal of,* vol. 48, pp. 1290-1301, 2013.

[8] C. Stagni, C. Guiducci, L. Benini, B. Riccò, S. Carrara, B. Samorí, *et al.*, "CMOS DNA sensor array with integrated A/D conversion based on label-free capacitance measurement," *Solid-State Circuits, IEEE Journal of,* vol. 41, pp. 2956-2964, 2006.

[9] E. Ghafar-Zadeh and M. Sawan, "A hybrid microfluidic/CMOS capacitive sensor dedicated to lab-on-chip applications," *Biomedical Circuits and Systems, IEEE Transactions on*, vol. 1, pp. 270-277, 2007.

[10] J. M. Rothberg, W. Hinz, T. M. Rearick, J. Schultz, W. Mileski, M. Davey, *et al.*, "An integrated semiconductor device enabling non-optical genome sequencing," *Nature*, vol. 475, pp. 348-352, 2011.

[11] N. Sun, T.-J. Yoon, H. Lee, W. Andress, R. Weissleder, and D. Ham, "Palm NMR and 1-chip NMR," *Solid-State Circuits, IEEE Journal of*, vol. 46, pp. 342-352, 2011.

[12] M. Pellecchia, D. S. Sem, and K. Wüthrich, "NMR in drug discovery," *Nature Reviews Drug Discovery*, vol. 1, pp. 211-219, 2002.

[13] H. Lee, E. Sun, D. Ham, and R. Weissleder, "Chip–NMR biosensor for detection and molecular analysis of cells," *Nature medicine*, vol. 14, pp. 869-874, 2008.

[14] D. I. Hoult and R. Richards, "The signal-to-noise ratio of the nuclear magnetic resonance experiment," *Journal of Magnetic Resonance (1969)*, vol. 24, pp. 71-85, 1976.

[15] R. M. Fratila and A. H. Velders, "Small-volume nuclear magnetic resonance spectroscopy," *Annual Review of Analytical Chemistry*, vol. 4, pp. 227-249, 2011.

[16] http://www.chem.yorku.ca/NMR/NMRFacility.htm

[17] K. Hashi, S. Ohki, S. Matsumoto, G. Nishijima, A. Goto, K. Deguchi, K. Yamada, T. Noguchi, S. Sakai, and M. Takahashi, "Achievement of 1020MHz NMR," *Journal of Magnetic Resonance*, vol. 256, pp. 30-33, 2015.

[18] http://www.nims.go.jp/eng/news/press/2015/07/201507010.html

[19] D. Oligschläger, S. Lehmkuhl, J. Watzlaw, S. Benders, E. De Boever, C. Rehorn, *et al.*, "Miniaturized multi-coil arrays for functional planar imaging with a single-sided NMR sensor," *Journal of Magnetic Resonance*, vol. 254, pp. 10-18, 2015.

[20] http://www.magritek.com/products/terranova/

[21] J. D. Trumbull, I. K. Glasgow, D. J. Beebe, and R. L. Magin, "Integrating microfabricated fluidic systems and NMR spectroscopy," *Biomedical Engineering, IEEE Transactions on*, vol. 47, pp. 3-7, 2000.

[22] http://www.oxford-instruments.com/products/spectrometers/nuclear-magnetic-resonance-nmr

[23] https://www.bruker.com/products/mr/td-nmr/minispec-mq-series.html

[24] T. F. Kong, W. K. Peng, T. D. Luong, N.-T. Nguyen, and J. Han, "Adhesive-based liquid metal radio-frequency microcoil for magnetic resonance relaxometry measurement," *Lab on a Chip*, vol. 12, pp. 287-294, 2012.

[25] http://www.metrolab.com/products/pm1055/

[26] H. Wensink, F. Benito-Lopez, D. C. Hermes, W. Verboom, H. J. Gardeniers, D. N. Reinhoudt, and A. van den Berg, "Measuring reaction kinetics in a lab-on-a-chip by microcoil NMR," *Lab on a Chip*, vol. 5, pp. 280-284, 2005.

[27] A. McDowell and E. Fukushima, "Ultracompact NMR: 1 H spectroscopy in a subkilogram magnet," *Applied Magnetic Resonance*, vol. 35, pp. 185-195, 2008.

[28] C. I. Daniel, F. n. Vaca Chávez, G. Feio, C. A. Portugal, J. o. G. Crespo, and P. J. Sebastião, "1H NMR Relaxometry, Viscometry, and PFG NMR Studies of Magnetic and Nonmagnetic Ionic Liquids," *The Journal of Physical Chemistry B*, vol. 117, pp. 11877-11884, 2013.

[29] http://www.gmw.com/electromagnets/

[30] W. Gil, J. Bonn, O. Dormicchi, R. Gehring, J. Kleinfeller, A. Kosmider, *et al.*, "Status of the magnets of the two tritium pumping sections for KATRIN," *Applied Superconductivity, IEEE Transactions on*, vol. 22, pp. 4500604-4500604, 2012.

[31] http://www.as-g.it/

[32] J. C. Edwards, "A Review of Applications of NMR Spectroscopy in the Petroleum Industry," *Spectroscopic Analysis of Petroleum Products and Lubricants", K Nadkami, ed. ASTM International,* 2011.

[33] J. C. Edwards and P. J. Giammatteo, "Process NMR spectroscopy: Technology and on-line applications," *Process analytical technology; Bakeev K, Ed. 2nd ed. Chichester, UK: John Wiley & Sons,* pp. 303-332, 2010.

[34] http://www.nmr-design.com/products/nmr-relaxometer-mSpin

[35] http://www.jeolusa.com/HOME/tabid/174/Default.aspx

[36] http://www.spincore.com/products/Magnets/NMR-Permanent-Magnets.shtml

[37] D. Hoult, "The principle of reciprocity in signal strength calculations—a mathematical guide," *Concepts in Magnetic Resonance,* vol. 12, pp. 173-187, 2000.

[38] J. Anders, G. Chiaramonte, P. SanGiorgio, and G. Boero, "A single-chip array of NMR receivers," *Journal of Magnetic Resonance,* vol. 201, pp. 239-249, 2009.

[39] R. Beiranvand, "Analyzing the uniformity of the generated magnetic field by a practical one-dimensional Helmholtz coils system," *Review of Scientific Instruments,* vol. 84, p. 075109, 2013.

[40] P. Kędzia, T. Czechowski, M. Baranowski, J. Jurga, and E. Szcześniak, "Analysis of Uniformity of Magnetic Field Generated by the Two-Pair Coil System," *Applied magnetic resonance,* vol. 44, pp. 605-618, 2013.

[41] R. M. Fratila, M. V. Gomez, S. Sýkora, and A. H. Velders, "Multinuclear nanoliter one-dimensional and two-dimensional NMR spectroscopy with a single non-resonant microcoil," *Nature communications,* vol. 5, 2014.

[42] P. Van Bentum, J. Janssen, A. Kentgens, J. Bart, and J. Gardeniers, "Stripline probes for nuclear magnetic resonance," *Journal of Magnetic Resonance,* vol. 189, pp. 104-113, 2007.

[43] J. L. Markley, "NMR analysis goes nano," *Nature biotechnology,* vol. 25, pp. 750-751, 2007.

[44] Y. Maguire, I. L. Chuang, S. Zhang, and N. Gershenfeld, "Ultra-small-sample molecular structure detection using microslot waveguide nuclear spin resonance," *Proceedings of the National Academy of Sciences,* vol. 104, pp. 9198-9203, 2007.

[45] H. G. Krojanski, J. r. Lambert, Y. Gerikalan, D. Suter, and R. Hergenröder, "Microslot NMR probe for metabolomics studies," *Analytical chemistry,* vol. 80, pp. 8668-8672, 2008.

[46] T. Cherifi, N. Abouchi, G.-N. Lu, L. Bouchet-Fakri, L. Quiquerez, B. Sorli, *et al.*, "A CMOS microcoil-associated preamplifier for NMR spectroscopy," *Circuits and Systems I: Regular Papers, IEEE Transactions on,* vol. 52, pp. 2576-2583, 2005.

[47] J. Anders, P. SanGiorgio, and G. Boero, "A fully integrated IQ-receiver for NMR microscopy," *Journal of Magnetic Resonance,* vol. 209, pp. 1-7, 2011.

[48] N. Sun, Y. Liu, H. Lee, R. Weissleder, and D. Ham, "CMOS RF biosensor utilizing nuclear magnetic resonance," *Solid-State Circuits, IEEE Journal of,* vol. 44, pp. 1629-1643, 2009.

[49] K. Ehrmann, N. Saillen, F. Vincent, M. Stettler, M. Jordan, F. M. Wurm, P.-A. Besse, and R. Popovic, "Microfabricated solenoids and Helmholtz coils for NMR spectroscopy of mammalian cells," *Lab on a Chip,* vol. 7, pp. 373-380, 2007.

[50] K. Takeda, "OPENCORE NMR: Open-source core modules for implementing an integrated FPGA-based NMR spectrometer," *Journal of Magnetic Resonance,* vol. 192, pp. 218-229, 2008.

[51] V. Demas, J. L. Herberg, V. Malba, A. Bernhardt, L. Evans, C. Harvey, S. C. Chinn, R. S. Maxwell, and J. Reimer, "Portable, low-cost NMR with laser-lathe lithography produced microcoils," *Journal of Magnetic Resonance,* vol. 189, pp. 121-129, 2007.

[52] N. Sun, T.-J. Yoon, H. Lee, W. Andress, V. Demas, P. Prado, R. Weissleder, and D. Ham, "Palm NMR and one-chip NMR," in *Solid-State Circuits Conference Digest of Technical Papers (ISSCC), 2010 IEEE International*, 2010, pp. 488-489.

[53] P. Van Bentum, J. Janssen, A. Kentgens, J. Bart, and J. Gardeniers, "Stripline probes for nuclear magnetic resonance," *Journal of Magnetic Resonance*, vol. 189, pp. 104-113, 2007.

[54] M. H. Lam, M. A. Homenuke, C. A. Michal, and C. L. Hansen, "Sub-nanoliter nuclear magnetic resonance coils fabricated with multilayer soft lithography," *Journal of Micromechanics and Microengineering*, vol. 19, p. 095001, 2009.

[55] J. Anders and G. Boero, "A low-noise CMOS receiver frontend for MRI," in *Biomedical Circuits and Systems Conference, 2008. BioCAS 2008. IEEE*, 2008, pp. 165-168.

[56] S. S. Mohan, M. del Mar Hershenson, S. P. Boyd, and T. H. Lee, "Simple accurate expressions for planar spiral inductances," *Solid-State Circuits, IEEE Journal of*, vol. 34, pp. 1419-1424, 1999.

[57] S. S. Mohan, "The design, modeling and optimization of on-chip inductor and transformer circuits," 1999.

[58] A. Zolfaghari, A. Chan, and B. Razavi, "Stacked inductors and transformers in CMOS technology," *Solid-State Circuits, IEEE Journal of*, vol. 36, pp. 620-628, 2001.

[59] L. Lin, W.-Y. Yin, J.-F. Mao, and Y.-Y. Wang, "Implementation of new CMOS differential stacked spiral inductor for VCO design," *Microwave and Wireless Components Letters, IEEE*, vol. 17, pp. 727-729, 2007.

[60] N. Sun, Y. Liu, L. Qin, H. Lee, R. Weissleder, and D. Ham, "Small NMR biomolecular sensors," *Solid-State Electronics*, 2013.

[61] F. Bloch, "Nuclear induction," *Physical review*, vol. 70, p. 460, 1946.

[62] SDBSWeb : http://sdbs.db.aist.go.jp (National Institute of Advanced Industrial Science and Technology, date of access).

[63] A. Uddin, S. Yemenicioglu, C. Chen, E. Corigliano, K. Milaninia, and L. Theogarajan, "Integration of solid-state nanopores in a 0.5 μm CMOS foundry process," *Nanotechnology,* vol. 24, p. 155501, 2013.

[64] A. Rasmussen, M. Gaitan, L. E. Locascio, and M. E. Zaghloul, "Fabrication techniques to realize CMOS-compatible microfluidic microchannels," *Microelectromechanical Systems, Journal of,* vol. 10, pp. 286-297, 2001.

[65] D. Barrettino, M. Graf, W. H. Song, K.-U. Kirstein, A. Hierlemann, and H. Baltes, "Hotplate-based monolithic CMOS microsystems for gas detection and material characterization for operating temperatures up to 500 C," *Solid-State Circuits, IEEE Journal of,* vol. 39, pp. 1202-1207, 2004.

[66] I. Voiculescu, M. E. Zaghloul, R. A. McGill, E. J. Houser, and G. K. Fedder, "Electrostatically actuated resonant microcantilever beam in CMOS technology for the detection of chemical weapons," *Sensors Journal, IEEE,* vol. 5, pp. 641-647, 2005.

[67] E. Ghafar-Zadeh, M. Sawan, and V. P. Chodavarapu, "Micro-organism-on-chip: emerging direct-write CMOS-based platform for biological applications," *Biomedical Circuits and Systems, IEEE Transactions on,* vol. 3, pp. 212-219, 2009.